Stability analysis for n-periodic arrays of fluid systems

Article *in* Physical Review Fluids · November 2017

DOI: 10.1103/PhysRevFluids.2.113902

3 authors:

Peter Schmid
Imperial College London
208 PUBLICATIONS **5,566** CITATIONS
SEE PROFILE

Miguel Fosas de Pando
Universidad de Cádiz
14 PUBLICATIONS **41** CITATIONS
SEE PROFILE

Nigel Peake
University of Cambridge
153 PUBLICATIONS **1,361** CITATIONS
SEE PROFILE

Stability analysis for n-periodic arrays of fluid systems

Peter J. Schmid*

Department of Mathematics, Imperial College London,

London SW7 2AZ, United Kingdom

Miguel Fosas de Pando†

Department of Mechanical Engineering and Industrial Design,

University of Cádiz, 11519 Puerto Real, Spain

N. Peake‡

Department of Applied Mathematics and Theoretical Physics (DAMTP),

University of Cambridge, Cambridge CB3 0WA, United Kingdom

(Dated: October 19, 2017)

Abstract

A computational framework is proposed for the linear modal and nonmodal analysis of fluid systems consisting of a periodic array of n identical units. A formulation in either time or frequency domain is sought, and the resulting block-circulant global system matrix is analyzed using roots-of-unity techniques which reduce the computational effort to only one unit while still accounting for the coupling to linked components. Modal characteristics as well as non-modal features are treated within the same framework, as are initial-value problems and direct-adjoint looping. The simple and efficient formalism is demonstrated on selected applications, ranging from a Ginzburg-Landau equation with an n-periodic growth function to interacting wakes, to incompressible flow through a linear cascade consisting of 54 blades. The techniques showcased here are readily applicable to large-scale flow configurations consisting of n-periodic arrays of identical and coupled fluid components, as can be found, for example, in turbomachinery, ring flame-holders or nozzle exit corrugations. Only minor corrections to existing solvers have to be implemented to allow this present type of analysis.

* pjschmid@imperial.ac.uk

† miguel.fosas@uca.es

‡ n.peake@damtp.cam.ac.uk

I. INTRODUCTION

Fluid systems consisting of an array of identical sub-units are common in many industrial configurations. Prominent among them are high-performance axial or radial turbines, compressors or pumps where a specific number of blades are mounted on a circular hub. Other applications that fall under the same category are ring flame-holders in combustion chambers, injection devices in afterburners, or the corrugated aircraft-engine nacelles intended to diminish jet-induced noise. In these configurations the geometry of each individual sub-unit is identical, and so is the flow behavior in it (see figure 1 for an example and a sketch). Consequently, it seems tempting to analyze the flow through a single unit in isolation and account for the influence of neighboring components via periodic boundary conditions. While this practice has been widely applied, it is easy to demonstrate that it cannot capture a range of fluid motion (in particular, multi-modal fluid instabilities) that may be important for the safe and efficient operation of an n-periodic fluid device. More specifically, modal solutions that are periodic over the entire n units, but non-periodic over individual or multiple units, are excluded by a one-unit analysis with periodic boundary conditions.

A global analysis, i.e., treating the entire n-component geometry, would remedy this shortcoming, but would yield a discretized system of excessive, or even prohibitive, size. Although we will start our development from a formulation of the full global system, we will exploit its block-circulant structure to reduce it to a modified single-unit system, thus achieving the computational cost of isolated-unit periodic analyses while correctly modelling the full interaction with all $n-1$ sub-components. In addition, the breakdown into a single sub-unit and its subsequent linear analysis exhibits ideal scalability on a parallel computer architecture, demonstrating additional benefits for this type of analysis.

The ubiquity of fluid systems characterized by an n-periodic arrangement of identical units or by multi-periodic geometric features has spawned a great deal of analyses and simulations: flow in wavy or grooved channels [9, 15, 16, 40] or past arrays of roughness elements and vortex generators [6], acoustics in periodic wave-guides [1], energy extraction from an buoy array [12] and, of course, flow in turbomachines [8, 13, 14, 20, 23, 24, 30] and combustors [5, 28, 29, 31, 38, 39, 45] are but a few examples that fall under this category. Not surprisingly, specific analysis and simulation techniques that efficiently address this periodicity have been developed, in particular for turbomachinery applications,

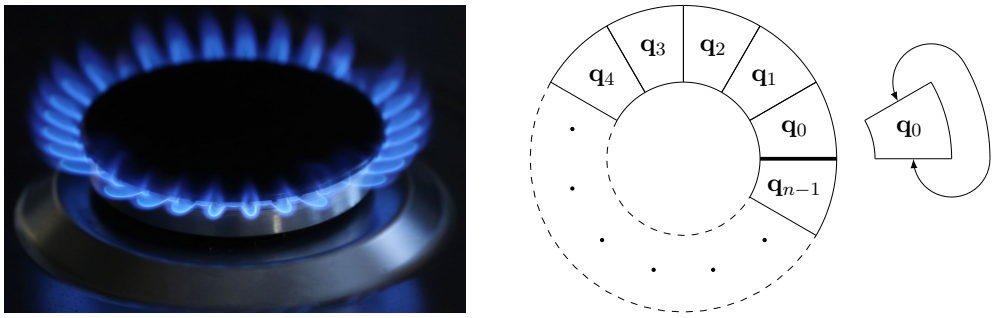

FIG. 1. (a) Example of an n-periodic fluid system: a gas-stove burner. (b) Sketch of an n-periodic fluid system consisting of n identical sub-units described by the respective state vector $\mathbf{q}_j,\ j = 0, \ldots, n-1$. (c) Analysis of a single unit with imposed periodic boundary conditions.

typically describing blade-to-blade dynamics, aeroelastic properties, and rotor-stator interactions. Among the proposed and frequently employed techniques are the harmonic-balance method [7, 17] which treats time-periodic flow as a sequence of matched frequencies, the phase-lagged boundary condition method [8] which employs phase-shifted flow variables on the interface between individual sub-units and, closely related, the chorochronic boundary condition method [13, 14, 23, 24] which generalizes the former techniques to multiple (and distinct) periodicity by an appropriate time-shift. In particular, the phase-lagged and chorochronic boundary conditions are commonly used in time-periodic flow, for example, in the periodic forcing of a turbomachinery blade passage by upstream stators or rotors. In this case, the implemented phase-shifts account for the time-delay in the forcing that the boundaries experience. The above techniques deal with a variety of geometric configurations and flow situations that exhibit a spatial (commonly azimuthal or discrete-rotational) periodicity, time-periodicity, or both.

Closest to the framework used in this article is the analysis of periodic systems using Bloch waves [4]. In a Bloch-wave formalism a relation between the solution in each sub-unit in the form of a geometric series is presumed. The geometric factor can be interpreted as a phase shift between solutions in various units, and is related to a cross-unit Bloch wavenumber. Substituting this ansatz into the governing equations yields a parameterized sequence of equations for the fundamental solution in a single unit [1, 28]; the parameter is the Bloch wavenumber.

In this article, we alternatively propose and use a linear-algebra approch, taking advan-

tage of the block-circulant nature of the linearized governing equations, for spectral analysis or initial-value problems. Among the well-known properties of block-circulant matrices is the analytic nature of the symbol curve [44], which takes on a particularly compact form for nearest-neighbor couplings that are often encountered in physical and engineering applications. This symbol curve can be computed without *a priori* committing to a specific number of individual sub-units. It is then discretized along its arclength according to the number n of sub-units which subsequently yields the spectrum of the n-periodic system. The discretized symbol curve represents the mapping of roots of unity under the respective block-matrices, where the indices of the roots correspond to the associated Bloch wavenumber. In addition to spectral (modal) properties, which mirror their equivalents in Bloch-wave theory, appropriate matrix functions, as used in a nonmodal stability/receptivity analysis, can also be formulated in a very compact manner, and the interaction between any two sub-units can be quantified and assessed, giving a measure of perturbation propagation across sub-units. The direct application of the formalism to matrix functions avoids the recasting into an eigenvalue problem, involving the adjoint operator. Lastly, rather than a reformulation of the governing equations using Bloch-wave theory, the proposed formalism can be straightforwardly implemented in existing simulation codes with little effort and minimal modifications.

The article is organized as follows. Starting from a full global description of an n-periodic fluid system, section II will introduce practical tools to arrive at a single-unit problem and to recover the complete global dynamics from solutions of this single unit. A range of analysis tools will be treated for modal (§ II A) and non-modal stability analyses (§ II B), impulse response, frequency response and inter-unit analyses (§ II C) and direct-adjoint looping (§ II D). Implementation strategies and access details to software used in this article are given in § II E. Section III gives demonstrations of the presented tools, starting with simple model equations and advancing to more complex and realistic configurations: a one-dimensional Ginzburg-Landau equation with an n-periodic growth potential (§ III A), a periodic array of interacting Bickley wakes (§ III B), and incompressible flow through an array of compressor blades (§ III C). In each application, particular attention is directed towards low-frequency organized motion and synchronization across multipe sub-units, which is contrasted to flow behavior periodic over one single unit. Lastly, section IV presents conclusions, extensions and an outlook for future applications.

II. MATHEMATICAL FRAMEWORK

We consider a general, nonlinear evolution problem of the form

$$\frac{\partial \mathbf{Q}}{\partial t} = \mathbf{f}(x, y, z, t; \mathbf{Q}) \tag{1}$$

where $\mathbf{Q}$ is a vector field that fully describes the state of our fluid system. We further assume periodicity over n identical units, which we representatively take in the z-coordinate. This periodicity is mathematically expressed in the form $\mathbf{f}(x, y, z, t; \mathbf{Q}) = \mathbf{f}(x, y, z + n\ell, t; \mathbf{Q})$ with ℓ as the z-extent of a single unit. After spatially discretizing the above equations and linearizing about an equilibrium point $\bar{\mathbf{Q}}$, with $\mathbf{Q} = \bar{\mathbf{Q}} + \varepsilon\mathbf{q}$, we arrive, for $\mathcal{O}(\varepsilon)$, at an evolution equation for the small perturbations $\mathbf{q}$ which reads

$$\frac{d}{dt}\mathbf{q} = \mathsf{A}\mathbf{q}, \tag{2}$$

with $\mathsf{A} = \partial\mathbf{f}/\partial\mathbf{Q}|_{\bar{\mathbf{Q}}}$ associated with (1). The specific n-periodic shape of the governing equations (1) results in a block-circulant form of the Jacobian A with

$$\frac{d}{dt}\begin{pmatrix} \mathbf{q}_0 \\ \mathbf{q}_1 \\ \vdots \\ \mathbf{q}_{n-2} \\ \mathbf{q}_{n-1} \end{pmatrix} = \underbrace{\begin{pmatrix} \mathsf{A}_0 & \mathsf{A}_1 & \cdots & \mathsf{A}_{n-2} & \mathsf{A}_{n-1} \\ \mathsf{A}_{n-1} & \mathsf{A}_0 & \cdots & \mathsf{A}_{n-3} & \mathsf{A}_{n-2} \\ \mathsf{A}_{n-2} & \mathsf{A}_{n-1} & \cdots & \mathsf{A}_{n-4} & \mathsf{A}_{n-3} \\ \vdots & \vdots & & \vdots & \vdots \\ \mathsf{A}_1 & \mathsf{A}_2 & \cdots & \mathsf{A}_{n-1} & \mathsf{A}_0 \end{pmatrix}}_{\mathsf{A}} \underbrace{\begin{pmatrix} \mathbf{q}_0 \\ \mathbf{q}_1 \\ \vdots \\ \mathbf{q}_{n-2} \\ \mathbf{q}_{n-1} \end{pmatrix}}_{\mathbf{q}}. \tag{3}$$

In the above expression, the discretized state vector $\mathbf{q}$ is partitioned into n components $\mathbf{q}_j,\ j = 0, \ldots, n-1$, each of which fully describing the flow in the j^{th} unit. By formulating the linearized problem in the form (3), we have tacitly assumed a coloring scheme for the state vector $\mathbf{q}$ that aligns all variables unit-by-unit and identically from unit to unit. Depending on the original formulation of (1) or the chosen time-stepping scheme an appropriate permutation of the state-vector variables may be required to bring the associated linearized system matrix A into block-circulant form; examples will be given in later sections.

It is important to note that formulation (3) allows interactions between a given unit j with *any* of the remaining units $i \neq j$. The matrix $\mathsf{A}_0 \in \mathbb{C}^{N\times N}$, along the diagonal of A describes the dynamics within the specific unit and is identical for each unit; the matrices $\mathsf{A}_{1,\ldots,n-1} \in \mathbb{C}^{N\times N}$, in the off-diagonal positions of A represent the interaction with the other units. The

number of degrees of freedom in each sub-unit is denoted by N (commonly, the number of grid points times the number of state variables). Owing to the n-periodic configuration, the global matrix A is block circulant. This specific shape will have consequences on the analysis and simulation of n-periodic fluid systems and will be further exploited in the following sections.

First and foremost, we are interested in bringing the block-circulant matrix A into block-diagonal form. Recalling that block-circulant matrices represent special cases of block-Toeplitz matrices whose spectrum can be described by its associated symbol [44], we form the matrix $\mathsf{J} \in \mathbb{C}^{n\times n}$ defined as $\mathsf{J}_{j+1,k+1} = \rho_j^k/\sqrt{n}$ with $j,k = 0,1,\ldots,n-1$, and ρ_j as the n^{th}-roots of unity according to

$$\rho_j = \exp(\mathrm{i}j\vartheta) \qquad \text{with} \qquad \vartheta = \frac{2\pi}{n} \qquad \text{and} \qquad j = 0,1,\ldots,n-1. \tag{4}$$

Based on the matrix J we compose the unitary matrix $\mathsf{P} \in \mathbb{C}^{nN\times nN}$ according to

$$\mathsf{P} = \mathsf{J} \otimes \mathsf{I}_{N\times N} \tag{5}$$

where $\otimes$ denotes the Kronecker product of two matrices and $\mathsf{I}_{N\times N}$ stands for the $N \times N$ identity matrix. With these definitions, it can easily be shown [18, 34] that a similarity transformation based on P block-diagonalizes the block-circulant matrix A according to

$$\mathsf{P}^H\mathsf{A}\mathsf{P} = \begin{pmatrix} \hat{\mathsf{A}}_0 & & & \\ & \hat{\mathsf{A}}_1 & & \\ & & \ddots & \\ & & & \hat{\mathsf{A}}_{n-1} \end{pmatrix} \equiv \hat{\mathsf{A}} \tag{6}$$

with $\hat{\mathsf{A}}_j \in \mathbb{C}^{N\times N}$ denoting the decoupled subsystem matrices and the superscript ^{H} representing the transconjugate (Hermitian) operation. More importantly, this expression can be employed to efficiently evaluate any matrix function $f(\mathsf{A})$ for a block-circulant A. We have

$$\mathsf{P}^H f(\mathsf{A})\mathsf{P} = \begin{pmatrix} f(\hat{\mathsf{A}}_0) & & & \\ & f(\hat{\mathsf{A}}_1) & & \\ & & \ddots & \\ & & & f(\hat{\mathsf{A}}_{n-1}) \end{pmatrix} = f(\hat{\mathsf{A}}), \tag{7}$$

which will be helpful in forming various matrix operators arising in the temporal and frequential analysis of n-periodic fluid systems (see below).

We can already state at this point that the evaluation of matrix functions – a key component in the analysis of fluid systems – has been reduced to a corresponding and independent analysis of n smaller subsystem matrices $\hat{\mathsf{A}}_{0,\ldots,n-1}$ by exploiting the block-circulant structure of the global system matrix A.

It is interesting to point out that only $\lfloor \frac{n}{2} \rfloor$, rather than n, computations are necessary, if the coupling matrices $\mathsf{A}_{j\neq 0}$ satisfy a symmetry condition of the form

$$\mathsf{A}_j^H = \mathsf{A}_{n-j}, \qquad\qquad j = 1, \ldots, n-1. \tag{8}$$

In this case, the influence of neighboring sub-units on each side of the central unit is equal. The symmetry condition (8) is often encountered in physical systems and is worth exploiting for computational efficiency.

In the above section and in what follows, we use the following notation for our system matrices: matrices associated with the full n-periodic (global) system will be denoted simply by a symbol, e.g., the matrix A; the various blocks of this block-circulant matrix will be denoted by a subscript $_j$, such as in A_j; once brought into block diagonal form via the matrix P, the transformed matrix will be marked by a caret, such as $\hat{\mathsf{A}}$, and its diagonal blocks will be indicated by $\hat{\mathsf{A}}_j$.

A. Modal solutions of the global matrix

A first step in our analysis is the assessment of the asymptotic ($t \to \infty$) stability of the global system matrix A, given by its spectrum. The block-diagonalization from the previous section suggests the spectral analysis of the diagonal blocks $\hat{\mathsf{A}}_j$, which can be accomplished independently and in parallel. The unitary similarity transformation (5) based on P is equivalent to the expression

$$\hat{\mathsf{A}}_j = \mathsf{A}_0 + \rho_j \mathsf{A}_1 + \rho_j^2 \mathsf{A}_2 + \cdots + \rho_j^{n-1} \mathsf{A}_{n-1} \tag{9}$$

for the decoupled subsystem matrices $\hat{\mathsf{A}}_j$ with the root-of-unity factor ρ_j introduced in (4) [42]. The spectrum of the global stability matrix A is then simply the union of the n spectra of $\hat{\mathsf{A}}_j$ for $j = 0, \ldots, n-1$.

By repeated multiplication by ρ_j of the eigenvalue problem associated with (3), it is not difficult to show that the compound vector of the form

$$\tilde{\mathbf{q}} = \begin{pmatrix} \mathbf{v}_j \\ \rho_j \mathbf{v}_j \\ \rho_j^2 \mathbf{v}_j \\ \vdots \\ \rho_j^{n-1} \mathbf{v}_j \end{pmatrix} \qquad j = 0, \ldots, n-1 \tag{10}$$

constitutes an eigenvector of $\mathsf{A} \in \mathbb{C}^{nN \times nN}$ i.e.,

$$\mathsf{A}\tilde{\mathbf{q}} = \tilde{\lambda}\tilde{\mathbf{q}}, \tag{11}$$

provided that the vector $\mathbf{v}_j \in \mathbb{C}^N$ in (10) satisfies the smaller $(N \times N)$ eigenvalue problem, involving the subsystem matrices $\hat{\mathsf{A}}_j$,

$$\hat{\mathsf{A}}_j \mathbf{v}_j = \lambda \mathbf{v}_j. \tag{12}$$

The geometric sequence for the eigenvector components, starting with a fundamental solution $\mathbf{v}_j$, is equivalent to the underlying assumption of Bloch-wave analysis.

We thus have a procedure to compute the full global spectrum without forming or decomposing the full global stability matrix A. For a given number n of identical sub-units, we start by computing the n^{th}-roots of unity $\rho_j, j = 0, \ldots, n-1$. For each of these roots, we form the matrix $\hat{\mathsf{A}}_j$ following (9) and solve for its eigenvalues $\Lambda_j = \text{diag}\{\lambda_1, \ldots, \lambda_N\}$ and eigenvectors $\mathsf{V}_j = \{\mathbf{v}_1, \ldots, \mathbf{v}_N\}$. We then form the global eigenvectors $\tilde{\mathbf{q}}$ from each $\mathbf{v}_{1,\ldots,N}$ according to (10); the eigenvalues $\lambda_{1,\ldots,N}$ for our specific value of ρ_j are already part of the global spectrum. As we repeat this procedure for all remaining roots-of-unity ρ_j, we recover the full global spectrum of A. However, only eigenvalue problems of the size of *one* individual unit (with N degrees of freedom) had to be solved, albeit multiple times. For large-scale applications, this latter feature becomes advantageous in a massively parallel computing environment.

The analysis of a single sub-unit with periodic boundary conditions amounts to an analysis of the stability matrix $\hat{\mathsf{A}}_0$ with $\rho_0 = 1$, i.e.,

$$\hat{\mathsf{A}}_0 = \sum_{i=1}^{n} \mathsf{A}_i. \tag{13}$$

Before proceeding it is important to recall that circulant matrices have orthogonal eigenvectors and are thus normal [44]. Consequently, the norm of any matrix function is determined by the least stable eigenvalue. For block-circulant matrices, as in our case, transient

effects can arise due to nonnormality of each individual sub-unit dynamics, but no additional transient effects arise from the superposition of different values of ρ_j as the eigenvectors of block-circulant matrices are block-orthogonal. This latter statement can easily be verified by forming the scalar product of two eigenvectors of the form (10). We assume that the two eigenvectors stem from two different values of ρ, which we take as ρ_j and ρ_k with $j \neq k$. Denoting by $\mathbf{v}_j$ an eigenvector of $\hat{\mathsf{A}}_j$ and by $\mathbf{v}_k$ an eigenvector of $\hat{\mathsf{A}}_k$ we arrive at

$$\tilde{\mathbf{q}}_j^H \mathsf{Q} \tilde{\mathbf{q}}_k = \begin{pmatrix} \mathbf{v}_j \\ \rho_j \mathbf{v}_j \\ \rho_j^2 \mathbf{v}_j \\ \vdots \\ \rho_j^{n-1} \mathbf{v}_j \end{pmatrix}^H \begin{pmatrix} \mathsf{Q}_0 & & & \\ & \mathsf{Q}_0 & & \\ & & \ddots & \\ & & & \mathsf{Q}_0 \end{pmatrix} \begin{pmatrix} \mathbf{v}_k \\ \rho_k \mathbf{v}_k \\ \rho_k^2 \mathbf{v}_k \\ \vdots \\ \rho_k^{n-1} \mathbf{v}_k \end{pmatrix} \tag{14a}$$

$$= (1 + \xi + \xi^2 + \cdots + \xi^{n-1}) \, \mathbf{v}_j^H \mathsf{Q}_0 \mathbf{v}_k \tag{14b}$$

$$= \frac{1 - \xi^n}{1 - \xi} \, \mathbf{v}_j^H \mathsf{Q}_0 \mathbf{v}_k \tag{14c}$$

with $\xi = \rho_j^* \rho_k = \exp(2\pi i (k-j)/n)$, and Q_0 representing a positive definite weight matrix defined over one sub-unit with $\mathsf{Q} = \mathrm{diag}\{\mathsf{Q}_0, \ldots, \mathsf{Q}_0\}$. Recalling that $\xi^n = 1$ for $j \neq k$, we conclude that two global eigenvectors corresponding to two different root-of-unity values are mutually Q_0-orthogonal. This eigenvector structure for block-circulant matrices A will be important for the nonmodal analysis in the next section.

B. Nonmodal solutions of the global matrix

Even though a spectral analysis of the n-periodic system gives insight into long-time stability properties, we are even more interested in the short- or finite-time dynamics that arises from a superposition of modal solutions. Two cases emerge: (i) the superposition of modal solutions within a single sub-unit, governed by the eigenstructure of $\hat{\mathsf{A}}_j$, and (ii) the superposition of modal solutions from *all* sub-units, taking into account the eigenstructures of $\hat{\mathsf{A}}_j, j = 0, \ldots, n-1$. The latter case is of particular interest, as it may described cross-unit dynamics which is absent in the former case.

A nonmodal analysis avoids the assumption of an exponential time-dependence $\exp(\lambda t)$ and, instead, considers the initial-value problem (2) or its driven counterpart [36]. We have

$$\begin{aligned} \frac{d}{dt}\mathbf{q} &= \mathsf{A}\mathbf{q}, & \frac{d}{dt}\mathbf{q} &= \mathsf{A}\mathbf{q}+\mathbf{f}, \\ \mathbf{q}(0) &= \mathbf{q}_0, & \mathbf{q}(0) &= \mathbf{0}. \end{aligned} \tag{15}$$

We define the maximum amplification $G(t)$ and the optimal frequency response $R(\omega)$ as follows

$$G(t) = \max_{\mathbf{q}_0} \frac{\|\mathbf{q}(t)\|}{\|\mathbf{q}_0\|} = \|\exp(t\mathsf{A})\| \qquad\qquad R(\omega) = \max_{\hat{\mathbf{f}}} \frac{\|\hat{\mathbf{q}}\|}{\|\hat{\mathbf{f}}\|} = \|(i\omega\mathsf{I}-\mathsf{A})^{-1}\| \tag{16}$$

with $\mathbf{f} = \hat{\mathbf{f}}\exp(i\omega t)$ and analogously for $\hat{\mathbf{q}}$. The matrix exponential norm determines the optimal amplification (in the chosen norm), starting from an optimal initial condition, over a user-defined time horizon $[0,\ t]$. The resolvent norm, in contrast, measures the optimal response (again, based on the chosen norm) to a harmonic forcing at a given frequency ω; the spatial shape of the optimal driving is given by $\hat{\mathbf{f}}$. Either analysis captures effects due to a potential non-orthogonality of the eigenvector structure or, equivalently, the non-normality of the underlying linearized evolution operator A.

In general, we have to evaluate the norm of a matrix function $\|f(\mathsf{A})\|$ (either $f(z) = \exp(tz)$ or $f(z) = (i\omega - z)^{-1}$ in our case) for block-circulant arguments A. An eigenvalue decomposition of A, using its block-circulant structure, will be used to accomplish this. First, we recall the weight matrix $\mathsf{Q}_0 \in \mathbb{R}^{N\times N}$, defined identically over each sub-unit, which expresses a particular, and physically meaningful, measure of state-vector size, as well as the matrix $\mathsf{Q} = \mathrm{diag}\{\mathsf{Q}_0,\ldots,\mathsf{Q}_0\}$ as the block-diagonal matrix consisting of the n individual weight matrices Q_0. The latter matrix is used to express the norm of the global state vector according to $\|\mathbf{q}\|_\mathsf{Q}^2 = \mathbf{q}^H\mathsf{Q}\mathbf{q}$. This weighted vector norm induces the corresponding matrix norm as follows: the positive definite matrix Q_0 is Cholesky-decomposed into $\mathsf{Q}_0 = \mathsf{F}_0^H\mathsf{F}_0$, and block-diagonal matrices are formed according to $\mathsf{F} = \mathrm{diag}\{\mathsf{F}_0,\ldots,\mathsf{F}_0\}$ and $\mathsf{F}^{-1} = \mathrm{diag}\{\mathsf{F}_0^{-1},\ldots,\mathsf{F}_0^{-1}\}$. The global matrix norm, applied to $f(\mathsf{A})$, is then given as $\|f(\mathsf{A})\|_\mathsf{Q} = \|\mathsf{F}f(\mathsf{A})\mathsf{F}^{-1}\|_2$, with the subscript $_2$ indicating the standard 2-norm [37]. We proceed by bringing the global matrix function of the block-circulant A into block-diagonal form using the unitary transformation P, as introduced in (5). We then deduce for the (weighted) Q-norm of the global matrix function $f(\mathsf{A})$

$$\|f(\mathsf{A})\|_\mathsf{Q} = \|\mathsf{F}\mathsf{P}f(\hat{\mathsf{A}})\mathsf{P}^H\mathsf{F}^{-1}\|_2 = \max_j \|\mathsf{F}_0\mathsf{V}_j f(\mathsf{\Lambda}_j)\mathsf{V}_j^{-1}\mathsf{F}_0^{-1}\|_2, \qquad j = 0,\ldots,n-1. \tag{17}$$

The eigenvalues and eigenvectors in (17) satisfy $\hat{\mathsf{A}}_j \mathsf{V}_j = \mathsf{V}_j \mathsf{\Lambda}_j$. The rightmost expression in (17) contains only matrices that are defined on a sub-unit, and equation (17) thus states that the Q-weighted norm of the global matrix function is simply the maximum over all sub-unit matrix-norm calculations. This general expression can now be applied to $f(\mathsf{A}) = \exp(t\mathsf{A})$ to treat initial-value problems, or to $f(\mathsf{A}) = (i\omega - \mathsf{A})^{-1}$ to investigate harmonically driven systems.

Besides the maximum energy amplification of an initial condition, or the maximum energy response due to harmonic forcing, we are often interested in the shapes of the optimal initial and terminal conditions, or, more importantly, the shapes of the optimal forcing and excited response. For linear time-invariant problems, this computation is often performed by a singular value decomposition of the matrix exponential (evaluated at a given time t_*) or the resolvent norm (evaluated at a given frequency ω_*). As before, we can take advantage of the block-circulant structure of the underlying matrix and apply the singular-value decomposition (or, parenthetically, any other matrix decomposition) of $f(\mathsf{A})$ to each of the n blocks $f(\hat{\mathsf{A}}_j)$ individually, taking into account the weighting by the matrices F_0 and F_0^{-1}. Introducing the singular-value decomposition of the decoupled blocks as $\mathsf{U}_j \mathsf{\Sigma}_j \mathsf{W}_j^H = \mathrm{svd}(\mathsf{F}_0 f(\hat{\mathsf{A}}_j) \mathsf{F}_0^{-1})$, we can cast the principal left and right singular vectors $\mathbf{u}$ and $\mathbf{w}$ of the (global) matrix $f(\mathsf{A})$ in the form

$$\mathbf{u} = \begin{pmatrix} \mathbf{u}_j \\ \rho_j \mathbf{u}_j \\ \rho_j^2 \mathbf{u}_j \\ \vdots \\ \rho_j^{n-1} \mathbf{u}_j \end{pmatrix} \qquad \mathbf{w} = \begin{pmatrix} \mathbf{w}_j \\ \rho_j \mathbf{w}_j \\ \rho_j^2 \mathbf{w}_j \\ \vdots \\ \rho_j^{n-1} \mathbf{w}_j \end{pmatrix} \tag{18}$$

with $\mathbf{u}_j$ and $\mathbf{w}_j$ as the principal left and right singular vectors of $f(\hat{\mathsf{A}}_j)$ and j chosen as $j = \mathrm{argmax}_j \sigma_j$ with σ_j as the largest singular value of $\mathsf{\Sigma}_j$. In other words, we select j as the index that yields the largest norm (maximum singular value) of $f(\hat{\mathsf{A}}_j)$ over all its values $j = 0, \ldots, n-1$. The above expressions then provide a procedure to compute the optimal perturbation and the optimal frequency response of the *global* n-periodic system by solving for the principal singular vectors of the n *local* subsystems. Moreover, the computations for the n subsystems are independent and can be readily parallelized.

C. Input-output analysis and cross-unit dynamics

It is often advantageous and instructive to assess the input-output behavior of a complex system. To this end, forcing is applied only to a specific subdomain of the flow or to only a particular state variable; likewise, only limited and user-specified output quantities are measured and assessed. In this manner, the strength and characteristics of a link between an input and output quantity can be probed, leading to more physical insight into the fluid system [22]. For example, the influence of fuel-mixture fluctuations in the feedpipe on the acoustic far-field output of a premixed flame could be quantified, to name a representative case from combustion dynamics for this type of analysis.

Within our block-circulant analysis framework, we are interested in evaluating the general expression, formulated for the global system,

$$K = \|\mathsf{C}f(\mathsf{A})\mathsf{B}\|_{\mathsf{Q}} \tag{19}$$

where B and C represent masking matrices that select and construct specific input and output quantities, respectively, from the global state vector. The matrix function $f(\mathsf{A})$ is either linked to an initial-value problem (via a fundamental solution operator or, for a linear time-invariant system, a matrix exponential) or a driven problem; see above. Exploiting the block-circulant structure of A we can bring the global matrix function into block-diagonal form using (5). We can write

$$K = \|\mathsf{FCP}f(\hat{\mathsf{A}})\mathsf{P}^H\mathsf{BF}^{-1}\|_2 \tag{20}$$

with $\hat{\mathsf{A}} = \mathrm{diag}\{\hat{\mathsf{A}}_0, \ldots, \hat{\mathsf{A}}_{n-1}\}$. At this stage we will be more specific and investigate the perturbation propagation across sub-units by choosing the block-diagonal masking matrices B and C to be non-zero in a specific sub-unit and zero elsewhere. More specifically, we study the dynamics between the single (input) sub-unit p and the single (output) sub-unit q. Within these sub-units we introduce the local masking matrices as $\mathsf{B}_p \in \mathbb{C}^{N\times N}$ and $\mathsf{C}_q \in \mathbb{C}^{N\times N}$, respectively. The global masking matrices (in block-diagonal notation) are then given as

$$\mathsf{B} = \begin{pmatrix} \mathsf{0}_{p-1} & & \\ & \mathsf{B}_p & \\ & & \mathsf{0}_{n-p} \end{pmatrix}, \qquad \mathsf{C} = \begin{pmatrix} \mathsf{0}_{q-1} & & \\ & \mathsf{C}_q & \\ & & \mathsf{0}_{n-q} \end{pmatrix} \tag{21}$$

where $\mathsf{0}_k$ denotes a $kN \times kN$ matrix of zeros. We further recall the definition (5) of the matrix P in terms of a Kronecker product which allows a more explicit formulation of $\mathsf{P}^H\mathsf{B}$ and CP by considering only nonzero contributions. We introduce the notation $\mathsf{M}_{:,p}$ and $\mathsf{M}_{q,:}$ to denote the p-th block-column or q-th block-row of a matrix M consisting of $n \times n$ blocks of size $N \times N$. We have

$$(\mathsf{P}^H\mathsf{B})_{:,\neq p} = \mathsf{0}_1 \qquad (\mathsf{P}^H\mathsf{B})_{:,p} = \mathsf{B}_p(\rho_k^{p-1})^*/\sqrt{n} \qquad k = 0, \dots, n-1, \tag{22a}$$

$$(\mathsf{CP})_{\neq q,:} = \mathsf{0}_1 \qquad (\mathsf{CP})_{q,:} = \mathsf{C}_q\rho_{q-1}^k/\sqrt{n} \qquad k = 0, \dots, n-1. \tag{22b}$$

Substituting this last expression into (20) yields the compact formula for the norm of a function $f(z)$, describing the trans-unit dynamics between unit p and q, according to

$$K_{pq} = \|\mathsf{FCP}f(\hat{\mathsf{A}})\mathsf{P}^H\mathsf{BF}^{-1}\|_2 = \|\mathsf{F}_0\mathsf{C}_q\left(\frac{1}{n}\sum_{j=0}^{n-1}\zeta_j f(\hat{\mathsf{A}}_j)\right)\mathsf{B}_p\mathsf{F}_0^{-1}\|_2 \tag{23}$$

with $\zeta_j = \exp(2\pi\mathrm{i}j(q-p)/n)$. As before, the final expression contains only components that describe single-unit characteristics; they can be evaluated efficiently and independently. At the same time, global effects spanning multiple units are captured by the above formula.

D. Direct-adjoint analysis

The previous algorithms for the computation of optimal initial condition and frequency response, using the respective matrix function $f(\mathsf{A})$, via a singular-value decomposition holds for linear time-invariant systems. Deviating from this restriction requires a more general approach, commonly involving direct and adjoint equations [36]. In this approach, we state a cost functional $\mathcal{J}$ to be optimized, such as optimal energy amplification, maximal response to forcing or optimal suppression of instabilities, among many other options. In general, the cost functional depends on the (global) state vector $\mathbf{q}$ and a control variable $\mathbf{f}$ (e.g., modeling boundary forcing); mathematically, we have $\mathcal{J} = \mathcal{J}(\mathbf{q}, \mathbf{f})$. Our optimization problem $\mathcal{J} \to \text{opt}$ is constrained by our governing equation (3) which we augment on the left by $\mathbf{f}$ which represents the application of control efforts. It can then be restated as an

unconstrained problem by introducing Lagrange multipliers or adjoint variables, denoted by $\mathbf{q}^+$, which will enforce the constraint from our governing equation. We obtain an augmented Lagrangian $\mathcal{L}$ in the form

$$\mathcal{L}(\mathbf{q}, \mathbf{q}^+, \mathbf{f}) = \mathcal{J}(\mathbf{q}, \mathbf{f}) - \left\langle \mathbf{q}^+, \frac{d}{dt}\mathbf{q} - \mathsf{A}\mathbf{q} - \mathbf{f} \right\rangle \tag{24}$$

with $\langle \mathbf{f}_1, \mathbf{f}_2 \rangle = \int_0^T \mathbf{f}_1^H \mathbf{f}_2 \, dt$ as the chosen inner product. Rendering zero the first variations of $\mathcal{L}$ with respect to $\mathbf{q}, \mathbf{q}^+$ and $\mathbf{f}$, respectively, results in a system of three equations:

$$\frac{d}{dt}\mathbf{q} = \mathsf{A}\mathbf{q} + \mathbf{f}, \qquad -\frac{d}{dt}\mathbf{q}^+ = \mathsf{A}^H\mathbf{q}^+ + \frac{\delta \mathcal{J}}{\delta \mathbf{q}}, \qquad \frac{\delta \mathcal{J}}{\delta \mathbf{f}} = \mathbf{q}^+. \tag{25}$$

The first equation restates our original governing system, while the second equation represents an evolution equation for the adjoint variable $\mathbf{q}^+$. The third part of (25) produces an expression for the gradient of our cost functional $\mathcal{J}$ with respect to the control variable $\mathbf{f}$ and is referred to as the optimality condition. These three equations need to be satisfied for an optimal solution. Instead of solving the system of equations (25) simultaneously, we employ an iterative scheme: starting with an initial guess for $\mathbf{f}$, we solve the direct and adjoint equations in (25); the resulting solution is used to evaluate the optimality condition and, via the gradient expression, determine an improved guess for $\mathbf{f}$ for a subsequent iteration. The iterative scheme terminates after a user-defined convergence criterion is satisfied. For further details on the algorithmic steps, the reader is referred to [36] or [25].

Again, taking advantage of the block-circulant structure of A and A^H we can decouple the sub-units by using the transformation P from (5). Applying this transformation, we arrive at systems of three equations – the direct and adjoint evolution equation, as well as the optimality condition – for each of our sub-units. We obtain

$$\frac{d}{dt}\mathbf{q}_j = \hat{\mathsf{A}}_j\mathbf{q}_j + \mathbf{f}_j, \qquad -\frac{d}{dt}\mathbf{q}_j^+ = \hat{\mathsf{A}}_j^H\mathbf{q}_j^+ + \frac{\delta \mathcal{J}}{\delta \mathbf{q}_j}, \qquad \frac{\delta \mathcal{J}}{\delta \mathbf{f}_j} = \mathbf{q}_j^+ \tag{26}$$

with $(\mathbf{f}_0, \ldots, \mathbf{f}_{n-1}) = \mathsf{P}^H\mathbf{f}$. As before, these systems are best treated iteratively: the direct and adjoint evolution equations are solved for a given control $\mathbf{f}_j$ (a guess for the first iteration), after which the gradient expression is used to update/improve the control $\mathbf{f}_j$ for the next iteration. Once more, the global problem breaks down into n local problems, which can be solved independently.

E. Implementation for large-scale applications

The computational formalism for the analysis of n-periodic fluid systems based on the spectral properties of block-circulant matrices has been formulated for a first-order temporal evolution problem. Time-discretization by higher-order stepping schemes, however, typically introduces multiple time-levels of state vector. In this case, the corresponding spectral problem is polynomial in the eigenvalue, and the solution algorithm for the eigenvalues and eigenvectors has to be adjusted accordingly [27, 43]. It also has to be kept in mind that, in this case, the state vector has to be reordered to yield a unit-by-unit composition; the same reordering will bring the global system matrices into block-circulant form. An example where this modification is necessary is included below (see § III C).

For large-scale problems, the linearization step resulting in (2) can most conveniently be accomplished using techniques such as the complex-step derivative [26] combined with a tiling method based on the decoupling of grid-points beyond the maximum stencil width [32]. Automatic differentiation techniques (see [19]) can also be applied to access linearized or adjoint information, as can alternative techniques (see, e.g., [10]).

The case of nearest-neighbor coupling is rather common in many applications. In this case, only a three-unit system needs to be discretized and processed — independent of the final configuration and periodicity of interest. In other words, only the system matrices A_0, A_1 and A_2 (from the 3-periodic system) have to be formed and stored. Stability and receptivity properties of different configurations with a *varying* number of sub-units do not require additional computations beyond the initial three system matrices $\mathsf{A}_{0,1,2}$. Their superposition and weighting with ρ_j according to

$$\hat{\mathsf{A}}_j = \mathsf{A}_0 + \rho_j \mathsf{A}_1 + \mathsf{A}_2/\rho_j \tag{27}$$

determine the block-diagonalized sub-unit matrices $\hat{\mathsf{A}}_j$ that enter the expressions for the analysis of n-periodic systems given above. In more mathematical terms, the symbol curve is given as [44]

$$\hat{\mathsf{A}}(z) = \mathsf{A}_0 + z\mathsf{A}_1 + \mathsf{A}_2/z \tag{28}$$

for $z = \exp(i\theta)$ and $\theta \in [0,\ 2\pi]$, and θ-parameterized line-spectra can be computed as $\mathrm{eig}(\hat{\mathsf{A}}(\theta))$. The spectra for specific n-periodic configurations consist simply of discretizations of the unit circle $\exp(i\theta)$ into n points, i.e. $\exp(i\theta_j)$ with $\theta_j = 2\pi j/n$, and a subsequent

mapping onto the line-spectra (see figure 2 for a sketch). In this manner, it is straightforward to quantify the sensitivity of spectral properties to the removal ($n \to n-1$) or augmentation ($n \to n+1$) by a sub-unit. Treating the change in n as a matrix perturbation problem for $\hat{\mathsf{A}}(\exp(i\theta))$, we can link, to first order, a change in θ to a change in an eigenvalue of $\hat{\mathsf{A}}$ according to

$$\delta\lambda_k = i\mathbf{w}_k^H \left(\mathsf{A}_1 \exp(i\theta) - \mathsf{A}_2 \exp(-i\theta)\right) \mathbf{v}_k \; \delta\theta \tag{29}$$

where $\mathbf{w}_k, \mathbf{v}_k$ denote the left and right eigenvectors, respectively, of $\hat{\mathsf{A}}(\exp(i\theta))$ corresponding to the eigenvalue λ_k and satisfying the normalization condition $\mathbf{w}_k^H \mathbf{v}_k = 1$. For the special case of changing the number of sub-units from n to $n+\Delta$, we obtain for a user-defined root-of-unity j the expression $\delta\theta_j/\theta_j = -\Delta/(n+\Delta)$. From the above we can determine, for example, the change in growth rate of the k-th eigenvalue for a specific j by considering the real part of (29).

In an effort to encourage experimentation with the proposed computational framework and to facilitate the analysis of n-periodic fluid systems, the codes underlying the examples in this article (see § III) will be made available, together with a brief documentation.

III. APPLICATIONS

The methodology introduced above is now applied to n-periodic fluid systems of increasing complexity, starting from a simple model equation to the analysis of a 54-blade passage. In each subsection, various aspects of the formalism are demonstrated and special emphasis is directed towards effects stemming from a synchronization across multiple sub-units and the description of lock-in processes.

A. A simple model: the Ginzburg-Landau equation with periodic potential

In this first section, we will consider the linearized Ginzburg-Landau equation with a n-periodic potential or growth function. This equation models physical processes commonly encountered in more complex fluid systems, such as convection, dissipation, dispersion and localized amplification of perturbations. We have

$$\frac{\partial u}{\partial t} = -U\frac{\partial u}{\partial x} + \nu\frac{\partial^2 u}{\partial x^2} + \mu(x)u \tag{30}$$

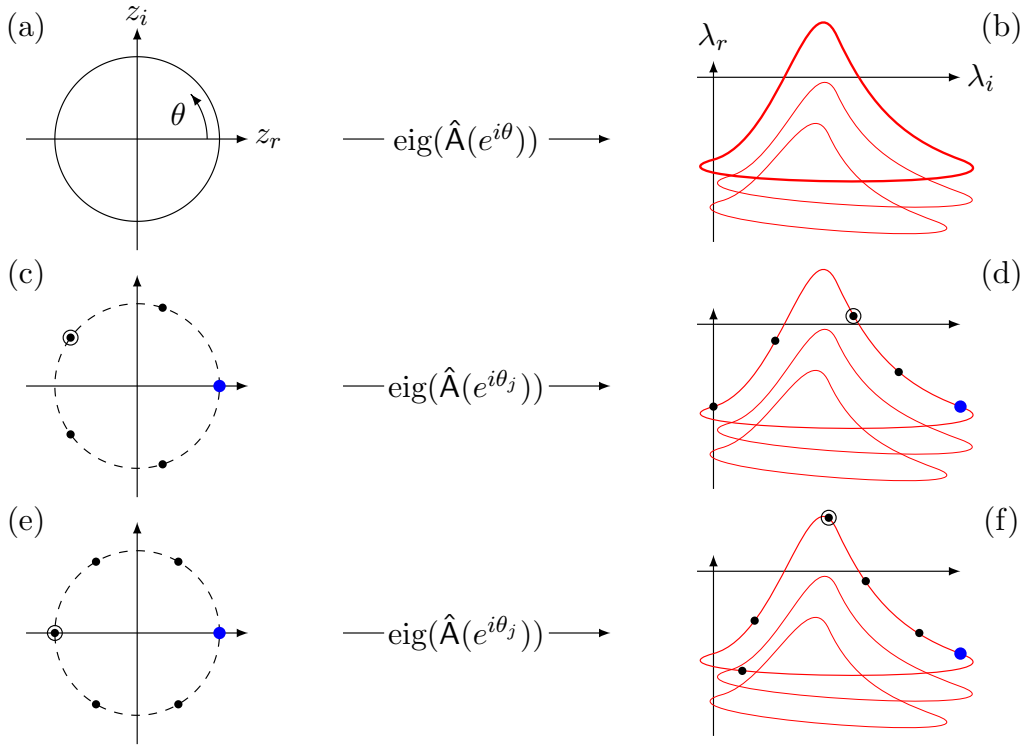

FIG. 2. Sketch of the spectrum of a block-circulant matrix. (a,b) The spectrum is continuously parameterized by θ; it is given by the map of the unit circle under $\mathrm{eig}(\hat{\mathsf{A}})$. N curves (in our sketch, $N = 3$) result, with $\hat{\mathsf{A}} \in \mathbb{C}^{N\times N}$. (c,d) The spectrum for a 5-periodic configuration, with block-matrices $\mathsf{A}_{0,1,n-1}$ as in (a,b), follows from a discretization of the continuous curve (only the dominant branch is shown). (e,f) The spectrum for a 6-periodic configuration, with block-matrices $\mathsf{A}_{0,1,n-1}$ as in (a,b). Notice the increase in growth rate of the least stable mode (circled symbol), as one more unit is added to the 5-periodic configuration. The eigenvalue corresponding to $\theta = 0$ is indicated in blue and is independent of the number n of sub-units.

with U as the advection speed, ν as the (potentially complex) viscosity and $\mu = -\cos(2\pi x)$ as the growth/decay function. We consider the interval $x \in [0,\ 1]$ for each sub-unit, but align n such units before periodic boundary conditions link the n-th unit back to the first one. The global problem thus spans the spatial interval $x \in [0,\ n]$. The continuous equation is discretized in space using finite differences, with $N = 100$ points per sub-unit interval. For the case presented below, we have chosen eleven identical sub-units, i.e., $n = 11$ (see figure 3 for a sketch of the global growth/decay function). The remaining governing parameters are $U = 10$ and $\nu = 10^{-4}$. This configuration models, for example, shear flow over a grooved

wall, where each shallow cavity acts as an amplifier of local instabilities. Of interest in this case is the global behavior of flow over an array of grooves, in particular the rise of synchronized motion linking multiple cavity units.

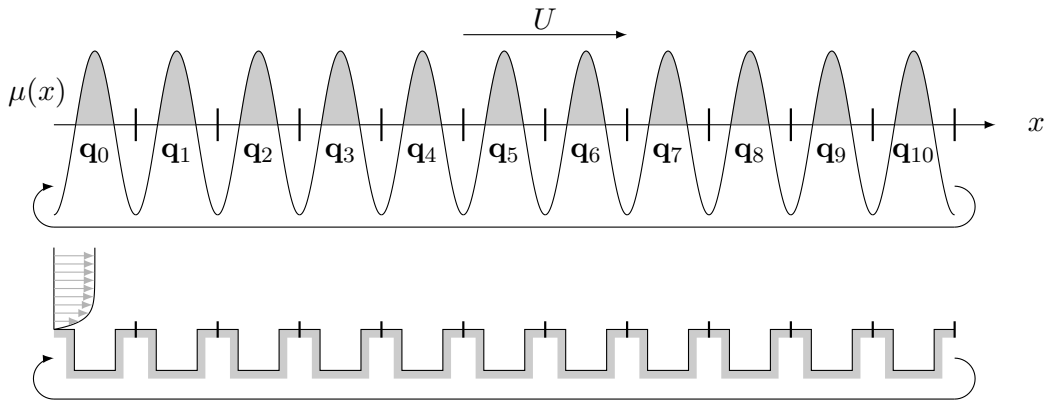

FIG. 3. Sketch of the 11-periodic potential (growth/decay function) used in the example of the Ginzburg-Landau equation, modelling the flow over a grooved wall (see bottom). The remaining parameters are $U = 10$ and $\nu = 10^{-4}$. Each of the 11 sub-units has been discretized by $N = 100$ mesh points.

First, we compute the spectrum, illustrated in figure 4(a). It shows an eigenvalue distribution typical of an advection-diffusion equation. Marked in figure 4(a) are the eigenvalues of the global problem, i.e., the eigenvalues of A, in blue symbols; they have been included to validate the collective eigenvalues of the submatrices $\hat{\mathsf{A}}_j, j = 0, \ldots, 10$; see the small black symbols. In addition, the eigenvalues of the matrix $\hat{\mathsf{A}}_0$ are included as red symbols. The latter eigenvalues represent the dynamics of the 1-periodic system: these eigenvalues result from considering a single sub-unit with periodic boundary conditions. We observe that the $\hat{\mathsf{A}}_0$-eigenvalues are more damped; the most unstable modes of the system, however, do not belong to the spectrum of the 1-periodic system.

An even more striking picture emerges from considering the response of the global and 1-periodic system to external harmonic forcing, see figure 4(b). We observe strong pseudo-resonance behavior for lower frequencies (e.g., $-20 \lesssim \omega \lesssim 20$), where the 1-periodic solution (in red) predicts an only modest response. We conclude that the inclusion of additional eigenvalues in the global spectrum is responsible for a slow-motion dynamics that spans and couples multiple sub-units — and thus is absent in the 1-periodic system.

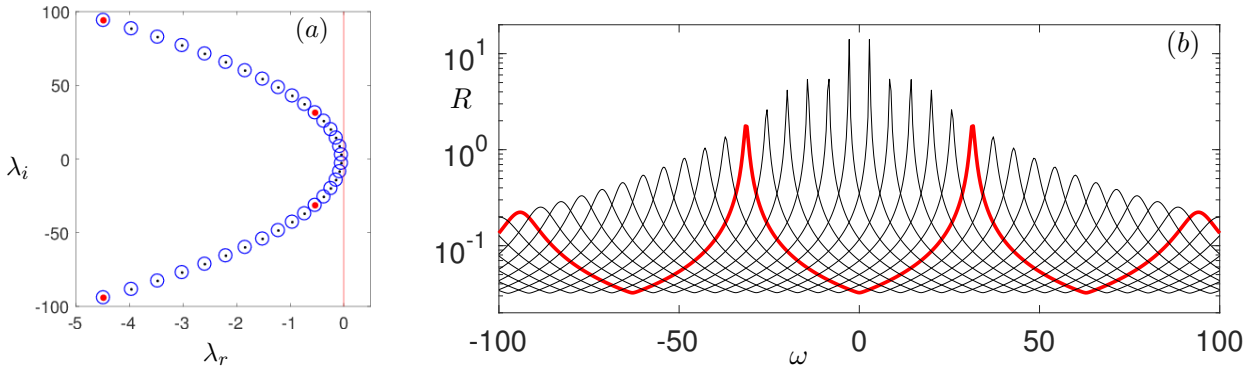

FIG. 4. Block-circulant complex Ginzburg-Landau system with $N = 100$ (discretization points per period), $\nu = 10^{-4}$, $U = 10$ and $\mu(x) = -\cos(2\pi x)$ with $x \in [0,\ 1]$. Eleven periods have been considered ($n = 11$). (a) Spectrum of the Ginzburg-Landau operator; the blue/black symbols indicate the global spectrum, computed globally (blue circles) and using the root-of-unity formalism (black dots). The red symbols correspond to the 1-periodic system ($\rho_0 = 1$), where periodic boundary conditions are enforced over one single sub-unit. (b) Resolvent norm R versus the forcing frequency ω; the black curves stem from the analysis of the subsystems for different ρ_j. The maximum over all curves corresponds to the global 11-periodic solution. The red curve corresponds to the choice $\rho_0 = 1$.

B. An n-periodic array of wakes

Whereas the periodicity of the previous example has been in the coordinate direction that is aligned with the mean advection, we will next consider the effect of a transverse periodicity on the collective behavior of n identical sub-units. Configurations with this type of multiple, but identical units are common in many fluid devices: spray nozzles, fuel injection systems, heat exchangers and screens are examples of this kind. Also, many geometric modifications to standard configurations, such as, e.g., the chevron-type corrugations of engine nacelles in commercial airliners to reduce noise, introduce a transverse periodicity of the mean-flow profiles.

In an attempt to model transverse periodic arrays of fluid systems we consider the linear stability of a row of wakes, where each individual unit is modelled as a Bickley wake with a base profiles given by

$$U(y) = 1 - A\ \mathrm{sech}^2\left[a\left(y - \frac{1}{2}\right)\right] \tag{31}$$

with $0 \leq y \leq 1$. The parameter a controls the width of the wake; the parameter A determines

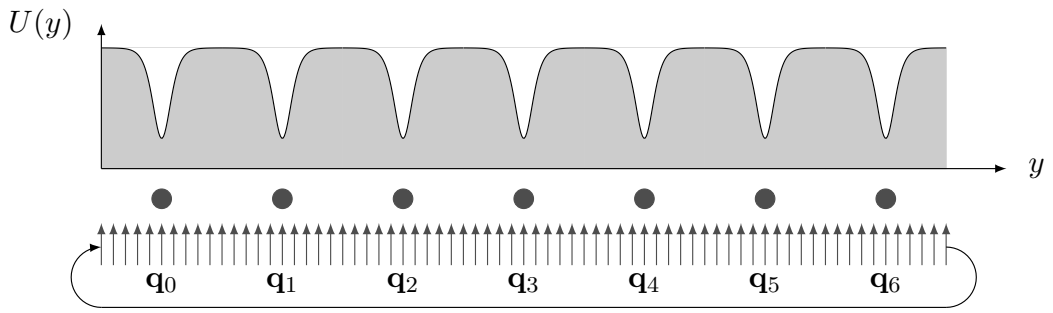

FIG. 5. Sketch of a 7-periodic configuration of Bickley wakes.

the velocity deficit. Both parameters can be used to model the streamwise evolution of the wake profile behind bluff bodies. In the examples below, we select $a = 10$ and $A = 0.75$. A global configuration consisting of n linked sub-units will be considered; a sketch of the configuration (for $n = 7$) is given in figure 5.

The temporal evolution of two-dimensional perturbations superimposed on this base flow is governed by the Orr-Sommerfeld equation given by

$$\lambda\left(\frac{d^2}{dy^2}-\alpha^2\right)v = -i\alpha U\left(\frac{d^2}{dy^2}-\alpha^2\right)v + i\alpha U''v + \frac{1}{Re}\left(\frac{d^2}{dy^2}-\alpha^2\right)^2 v \tag{32}$$

with v as the normal velocity, α as the streamwise wavenumber, Re as the Reynolds number based on the freestream velocity and the distance between the individual wakes, and λ as the eigenvalue whose real part constitutes the exponential growth or decay rate. The perturbation is assumed in the form $v(y)\exp[i\alpha x]\exp[\lambda t]$. Formulating the stability problem for a global problem consisting of n sub-units, a block-circulant global stability matrix results. As before, we are interested in contrasting the dynamics of perturbations over one sub-unit against the disturbance dynamics over multiple units. To this end, we deduce the entries in the block-circulant global matrix with nearest-neighbor coupling, i.e., A_0, A_1 and A_{n-1}, where A_0 describes the dynamics of the individual sub-unit while A_1 and A_{n-1} account for the coupling to adjacent units. We use fourth-order compact difference schemes to discretize equation (32) in the cross-stream coordinate direction.

First, we choose a Reynolds number of $Re = 200$, a streamwise wavenumber of $\alpha = 1$ and consider a configuration with three identical units. The spectrum is shown in figure 6(a) and indicates an asymptotic instability at these parameter values, with the least stable eigenvalue at $\lambda = 0.0993 + 0.9012i$. The eigenvalues are colored by the index j with $j = 0$ (representing a fully periodic state, $\rho_0 = 1$) in grey and $j = 1$ (representing a cross-unit periodicity,

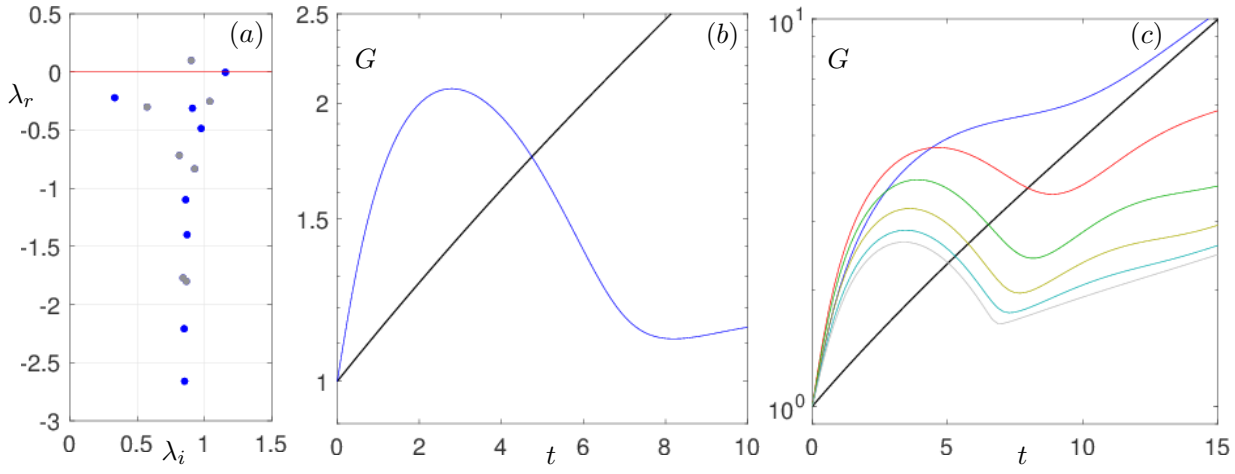

FIG. 6. (a) Spectrum of a three-unit configuration of Bickley wakes ($a = 10, A = 0.75$) with $\alpha = 1$ and $Re = 200$; in grey: $\rho_0 = 1$, in blue $\rho_1 = \exp(2\pi i/3)$. (b) Norm of the matrix exponential (maximal amplification) for the three-unit configuration. (c) Norm of the matrix exponential for a thirteen-unit configuration for $\alpha = 1$ and $Re = 200$ for $\rho_j,\ j = 0, \ldots, 6$.

$\rho_1 = \exp(2\pi i/3)$) in blue. We observe that the strongest instability is of the fully-periodic type; a nearly neutral, multi-unit-periodic mode, at a higher phase velocity λ_i/α, is the second-most amplified mode. For higher modes the spectrum displays the typical Y-shape of viscous shear flows: mean-modes aligned with the average base-flow velocity ($\bar{U} \approx 0.82$), which divide the spectrum into slower and faster modes. Modes with different periodicity interlace.

Depicting the modal shapes of the first six least stable modes gives more insight into the perturbation dynamics of the coupled three-wake configuration. This dynamic becomes more lucid by integrating streak-lines based on the six separate normal-velocity fields to indicate the cross-stream displacement of the perturbations. To this effect, an equispaced (in the y-direction) array of particles is released and tracked through the respective modal velocity field. The results are displayed in figure 7. For the least stable mode (figure 7(a)), we observe a synchronized oscillatory motion of the wake, depicted over a full period given by the respective eigenvalue (and ignoring the small imaginary part). The next most unstable mode (figure 7(b)), however, displays a non-synchronized behavior where the three wakes repeatedly diverge from and converge towards the adjacent units. This break in cross-stream symmetry continues for the next mode (figure 7(c)), but returns to symmetry for the fourth and fifth mode (figures 7(d,e)). The sixth mode in this sequence (figure 7(f)) again shows

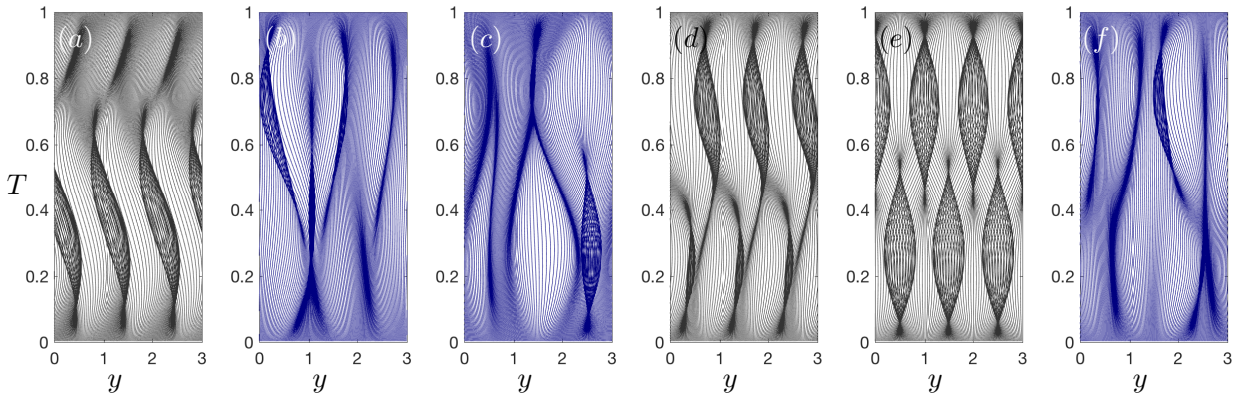

FIG. 7. Modal shapes of the first six least stable modes of the three-wake configuration, visualized by streak-lines integrated in the cross-stream velocity field. In grey: synchronized motion for $\rho_0 = 1$; in blue: unsynchronized motion for $\rho_1 = \exp(2\pi i/3)$. In all cases, a full period T, given by the respective phase velocity is shown; the real part of the eigenvalue has been ignored in the computation of the streak-lines.

unsynchronized sub-units.

While our analysis of the modal structures identifies the strongest instability for a synchronized motion (i.e., a mode with $\rho_0 = 1$), the finite-time analysis based on the matrix exponential norm shows (see figure 6(b)) that, for short times ($t \lesssim 4.5$), maximum amplification is achieved by an unsynchronized perturbation dynamics; for larger times ($t \gtrsim 4.5$), however, the synchronized motion prevails. The same graph demonstrates that unsynchronized transient amplification over two convective time units reaches energy levels that synchronized motion reaches only after more than six convective time units. Whether this disparity in amplification is sufficient for a selection principle and the observation of preferred (unsynchronized) structures requires additional consideration.

To further demonstrate the rise and importance of cross-unit motion, we extend the above analysis to a configuration with 13 units. This type of geometry may describe fluid motion past cylinder bundles or mesh screens. A modal analysis still confirms the least stable mode as a synchronized mode (with $\rho_0 = 1$, see figure 8(a)), the two subsequent modes, however, show the locking of adjacent units in groups (as displayed in figure 8(b,c) by streak-lines). The nonmodal analysis of the 13-wake configuration (figure 6(c)) based on the matrix exponential norm even more strongly asserts the fact that unsynchronized motion dominates the short-time dynamics of the 13-periodic array of Bickley wakes. For our parameter values,

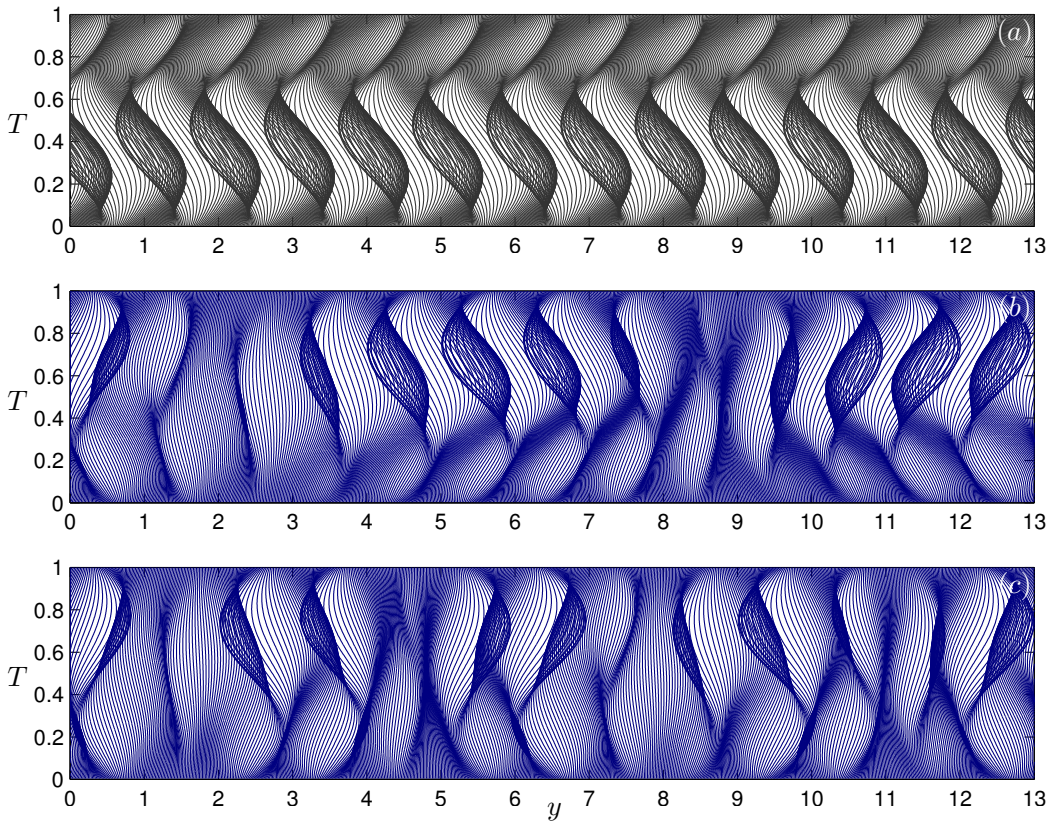

FIG. 8. Modal shapes of the first three least stable modes of a thirteen-wake configuration, visualized by streak-lines integrated in the cross-stream velocity field. In grey: synchronized motion for $\rho_0 = 1$; in blue: unsynchronized motion for $\rho_1 = \exp(2\pi i/13)$ and $\rho_2 = \exp(4\pi i/13)$. In all cases, a full period T, given by the respective phase velocity is shown; the real part of the eigenvalue has been ignored in the computation of the streak-lines.

the perturbation energy amplification from synchronized motion dominates only after more than 15 convective time units.

In closing, we stress that, besides considering the above temporal stability problem for the periodic array of Bickley wakes, the corresponding spatial stability problem can be treated within the same framework. In this case, a fourth-degree polynomial eigenvalue problem for the complex streamwise wavenumber α can be formulated that, after an appropriate reordering of the global state-vector $\mathbf{q}$, can be recast in block-circulant form.

C. Flow through a 54-periodic blade row

As a final example, we demonstrate the analysis of n-periodic fluid systems presented in this paper on a more complicated flow configuration of interest in turbomachinery applications. To this end, we consider the stability characteristics of incompressible flow through a periodic linear cascade.

Throughout this example we use a numerical solver for the two-dimensional Navier–Stokes equations that implements the projection-based immersed boundary method [41]. Based on this technique, the governing equations in nondimensional form formulated for a domain $\mathcal{D}$ read [33]

$$\frac{\partial \mathbf{u}}{\partial t} + \mathbf{u} \cdot \nabla \mathbf{u} = -\nabla p + \frac{1}{\mathrm{Re}} \nabla^2 \mathbf{u} + \int_{\mathcal{C}} \mathbf{f}(s) \delta(\mathbf{x} - \xi(s)) \, \mathrm{d}s, \tag{33}$$

$$\nabla \cdot \mathbf{u} = 0, \tag{34}$$

$$\mathbf{u}(\xi(s)) = \int_{\mathcal{D}} \mathbf{u}(\mathbf{x}) \delta(\xi(s) - \mathbf{x}) \, \mathrm{d}\mathbf{x} = \mathbf{u}_B(s) \qquad s \in \mathcal{C}, \tag{35}$$

where the pressure p and the distributed momentum sources $\mathbf{f}(s)$ along the boundary of the obstacle $\mathcal{C}$ act as a set of Lagrange multipliers that enforce, respectively, the incompressibility constraint and the no-slip boundary condition. The above equations are discretized using a staggered-mesh finite-volume formulation; the viscous terms are discretized using the implicit Crank–Nicolson method, the advection terms are discretized using the explicit second-order Adams–Bashforth scheme, and the integrals involving the delta functions are discretized using a mollified delta function [35]. At this point, the flow field at a given time step $\mathbf{Q}^{k+1}$ and the value of the Lagrange multiplier λ are obtained from the flow fields at the two previous time steps, denoted $\mathbf{Q}^k$ and $\mathbf{Q}^{k-1}$. Flow field boundary conditions $\mathbf{bc}_1$ and $\mathbf{bc}_2$ are imposed, and the following system of equations is solved:

$$\begin{pmatrix} \mathsf{A} & \mathsf{Q} \\ \mathsf{Q}^T & \mathsf{0} \end{pmatrix} \begin{pmatrix} \mathbf{Q}^{k+1} \\ \lambda \end{pmatrix} = \begin{pmatrix} \mathsf{B}\mathbf{Q}^k - \frac{3}{2}\mathcal{N}(\mathbf{Q}^k) + \frac{1}{2}\mathcal{N}(\mathbf{Q}^{k-1}) + \mathbf{bc}_1 \\ \mathbf{r}_2 \end{pmatrix}. \tag{36}$$

The reader is referred to [41] for the various definitions of the matrices A, B and Q, the nonlinear function $\mathcal{N}(\cdot)$ and the vectors $\mathbf{bc}_1, \mathbf{bc}_2$ and $\mathbf{r}_2$.

We now consider a two-dimensional periodic linear cascade consisting of 54 NACA E^3 Rotor B airfoils (see [3, 11] for a description of the blade geometry) with a pitch-to-chord ratio of $\sigma = H/C = 0.92936$ and a stagger angle of 56.6°. The governing equations are then

solved in the reference frame of the cascade; the velocity of the unperturbed incoming flow and the blade chord are taken, respectively, as the reference speed and reference length scale. The angle of attack, defined as the angle between the unperturbed incoming flow direction and the blade chord, is taken as 11.1°, and the Reynolds number Re, based on chord, is 700. The computational domain for one blade passage is defined for $-6.56 \leq x \leq 6.56$ and $-0.465 \leq y \leq 0.465$. Upstream of the blade passages we impose a Dirichlet boundary condition for the velocity components, while a convective outflow boundary condition is implemented downstream. In the horizontal direction, the numerical grid is uniform for $-0.55 \leq x \leq 0.55$, with $\Delta x = 0.0036$, and is stretched upstream and downstream until the maximum spacing is $\Delta x = 0.03$; in the vertical direction the numerical grid has a constant spacing equal to $\Delta y = 0.0036$. The time step has been taken as $\Delta t = 0.0018$ and the resulting numerical grid has 766 cells in the horizontal direction and 258 cells per blade passage in the vertical direction.

Following the remark in § II E about the efficient composition of the necessary matrices for nearest-neighbor configurations, we consider a three-blade passage to extract the sub-unit matrices required in our analysis.

First, the flow configuration presented above is found to be globally stable, and the base flow $\bar{\mathsf{Q}}$, depicted in figure 9 by the vertical velocity component, has been computed simply by marching in time the governing equations from a given initial condition. Note that the base flow is periodic over one blade passage.

The above nonlinear equations are linearized about the base flow presented above, yielding the following system of linear equations for the temporal advancement of a small perturbation $\mathbf{q}$ over one time step

$$\begin{pmatrix} \mathsf{A} & \mathsf{Q} \\ \mathsf{Q}^T & 0 \end{pmatrix} \begin{pmatrix} \mathbf{q}^{k+1} \\ \lambda \end{pmatrix} = \begin{pmatrix} (\mathsf{B} - \frac{3}{2}\mathsf{N})\mathbf{q}^k + \frac{1}{2}\mathsf{N}\mathbf{q}^{k-1} \\ \mathbf{0} \end{pmatrix}, \tag{37}$$

where $\mathsf{N} = (\partial \mathcal{N}(\mathbf{Q})/\partial \mathbf{Q})|_{\bar{\mathsf{Q}}}$ represents the linearized advection terms about the base flow $\bar{\mathsf{Q}}$. By introducing the following definition

$$\tilde{\mathbf{x}}^k = \begin{pmatrix} \mathbf{q} \\ \lambda \end{pmatrix}^k, \quad \tilde{\mathsf{M}} = \begin{pmatrix} \mathsf{A} & \mathsf{Q} \\ \mathsf{Q}^T & 0 \end{pmatrix}, \qquad \tilde{\mathsf{C}} = \begin{pmatrix} -\mathsf{B} + \frac{3}{2}\mathsf{N} & 0 \\ 0 & 0 \end{pmatrix} \quad \text{and} \quad \tilde{\mathsf{K}} = \begin{pmatrix} -\frac{1}{2}\mathsf{N} & 0 \\ 0 & 0 \end{pmatrix}, \tag{38}$$

the temporal advancement over one time step reads

$$\tilde{\mathsf{M}}\tilde{\mathbf{x}}^{k+1} + \tilde{\mathsf{C}}\tilde{\mathbf{x}}^k + \tilde{\mathsf{K}}\tilde{\mathbf{x}}^{k-1} = 0. \tag{39}$$

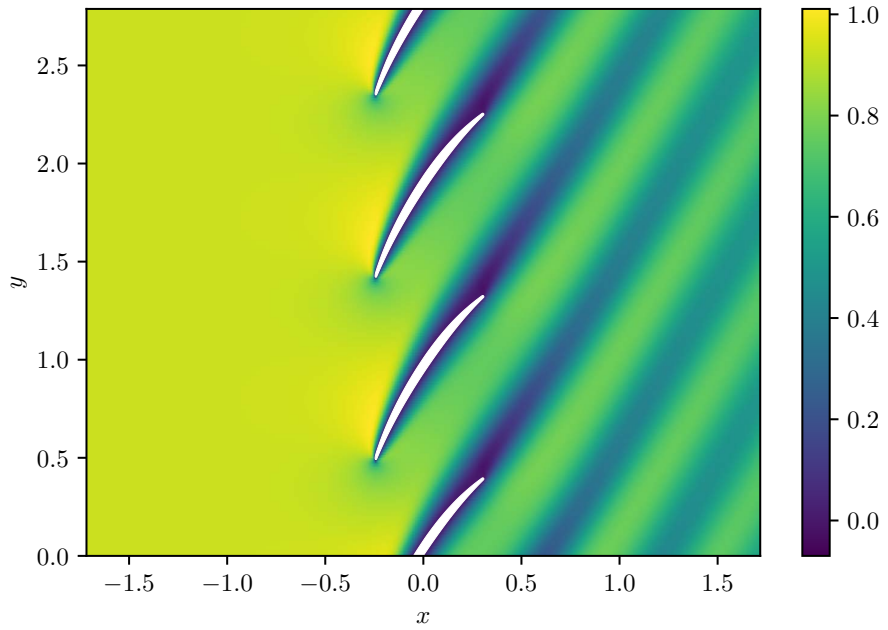

FIG. 9. Base flow for a linear cascade consisting of NACA E^3 Rotor B blade profiles with a pitch-to-chord ratio of $\sigma = H/C = 0.92936$ and a stagger angle of 56.6°. The angle of attack is 11.1° and the chord-based Reynolds number is $\mathrm{Re} = 700$. The flow is visualized by the vertical velocity component. See text for details on the numerical grid.

Considering (38), we note that while the matrix entries $\mathsf{A}, \mathsf{Q}, \mathsf{B}, \mathsf{N}$ are individually block-circulant, the matrices $\tilde{\mathsf{M}}, \tilde{\mathsf{C}}, \tilde{\mathsf{K}}$ are not. A final row reordering, which we introduce as a permutation G of a $3N \times 3N$ identity matrix, brings the state vector $\tilde{\mathbf{x}}$ into a unit-by-unit configuration, according to $\mathbf{x} = \mathsf{G}\tilde{\mathbf{x}}$. Applied to (38), we arrive at

$$\mathbf{x}^k = \mathsf{G}\tilde{\mathbf{x}}^k, \qquad \mathsf{M} = \mathsf{G}\tilde{\mathsf{M}}\mathsf{G}^T, \qquad \mathsf{C} = \mathsf{G}\tilde{\mathsf{C}}\mathsf{G}^T \quad \text{and} \quad \mathsf{K} = \mathsf{G}\tilde{\mathsf{K}}\mathsf{G}^T, \tag{40}$$

and the temporal advancement over one time step (now in block-circulant form) reads

$$\mathsf{M}\mathbf{x}^{k+1} + \mathsf{C}\mathbf{x}^k + \mathsf{K}\mathbf{x}^{k-1} = 0. \tag{41}$$

Following section II, we assess the long-time stability of the linearized dynamics by computing modal solutions of the global matrix. Introducing $\mathbf{x} = \hat{\mathbf{x}}e^{\lambda t}$ into equation (41), we arrive at the following quadratic eigenvalue problem

$$(\sigma^2\mathsf{M} + \sigma\mathsf{C} + \mathsf{K})\hat{\mathbf{x}} = 0 \qquad \sigma = e^{\lambda\Delta t}. \tag{42}$$

As stated before, the matrices M, C and K are block-circulant; therefore we introduce the n^{th} roots-of-unity ρ_j and express the eigenvector of the full system $\hat{\mathbf{x}}$ as

$$\hat{\mathbf{x}} = \begin{pmatrix} \hat{\mathbf{x}}_j \\ \rho_j \hat{\mathbf{x}}_j \\ \vdots \\ \rho_j^{n-2} \hat{\mathbf{x}}_j \\ \rho_j^{n-1} \hat{\mathbf{x}}_j \end{pmatrix}, \tag{43}$$

where $\hat{\mathbf{x}}_j$ satisfies a quadratic eigenvalue problem for a modified unit given by

$$\left(\sigma^2 \hat{\mathsf{M}}_j + \sigma \hat{\mathsf{C}}_j + \hat{\mathsf{K}}_j\right) \hat{\mathbf{x}}_j = 0 \qquad j = 0, \ldots, n-1, \tag{44}$$

and

$$\hat{\mathsf{M}}_j = \mathsf{M}_0 + \rho_j \mathsf{M}_1 + \mathsf{M}_2/\rho_j \tag{45a}$$

$$\hat{\mathsf{C}}_j = \mathsf{C}_0 + \rho_j \mathsf{C}_1 + \mathsf{C}_2/\rho_j \tag{45b}$$

$$\hat{\mathsf{K}}_j = \mathsf{K}_0 + \rho_j \mathsf{K}_1 + \mathsf{K}_2/\rho_j \tag{45c}$$

with $\mathsf{M}_{0,1,2}, \mathsf{C}_{0,1,2}, \mathsf{K}_{0,1,2}$ extracted from the 3-periodic system (40).

The above eigenvalue problems have been solved using the software package `SLEPc` [21] together with the sparse direct solver `MUMPS` [2] and the shift–invert technique. The spectrum of the operator has been computed for different shift values and is shown in figure 10(a–c). More specifically, we display the continuously parameterized symbol curves, as defined by equation (28). These curves describe the spectrum in the limit of an infinite system, without any *a priori* decision on a specific number of individual units. The computations are performed on a three-blade passage system. Figure 10(a) clearly displays line spectra, parameterized by an angle $\theta \in [0,\ 2\pi]$, which represent the mapping of the unit circle $z = \exp(i\theta)$ under the nearest-neighbor coupled system. The largest modal growth is achieved for frequencies of $\lambda_i \sim 4.8$, but a preference of very low-frequency modes ($\lambda_i \sim 0.1$) is also expected due to a weak damping of these structures. Figures 10(b,c) highlight these important parts of the spectrum, and show a "discretization" of these continuously parameterized, spectral lines – given by selecting $n = 54$ units. Based on the line spectra, we can assess the sensitivity of the system to the number of individual units, estimate the number of units for weakest modal damping (or largest modal amplification) and predict the Bloch wavelength (root of unity) of this least-damped/most-amplified structure.

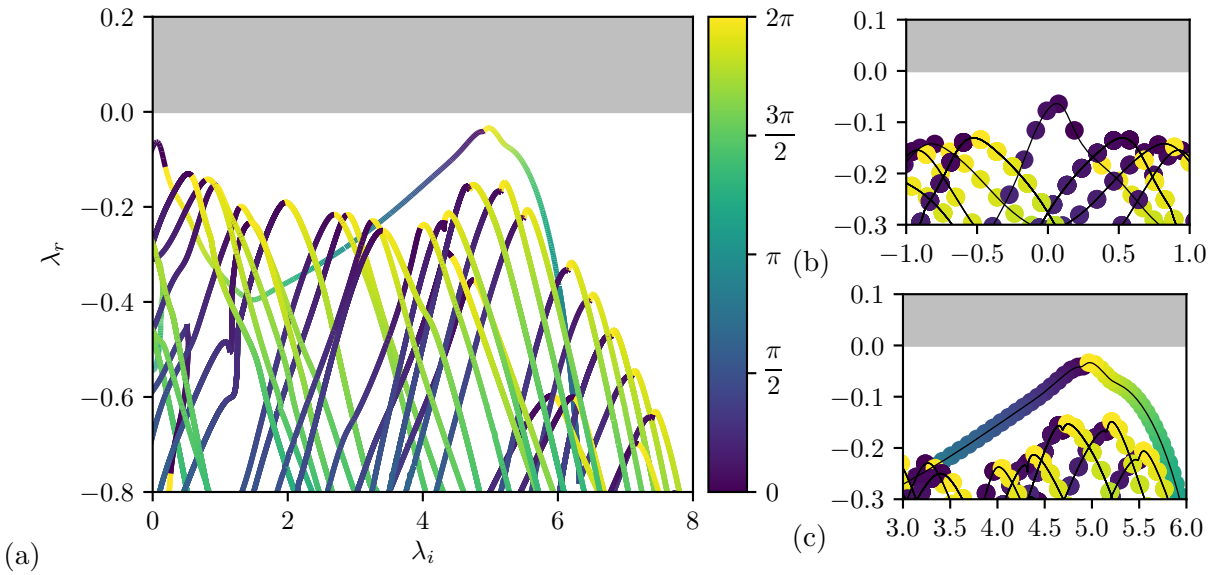

FIG. 10. Continuously parameterized spectrum describing the dynamics of perturbations for a linear cascade; the vertical axis represents the temporal growth rate λ_r and the horizontal axis indicates the angular frequency λ_i. (a) The line spectra are colored by the angle $\theta \in [0,\ 2\pi]$, parameterizing the unit circle $z = \exp(i\theta)$ in equation (28). (b,c) Zoom-in on the least-damped regions, and discretization of the continuously parameterized symbol curves by selecting $n = 54$ blade passages (depicted in full circles).

As an example of a nonmodal analysis in n-periodic fluid systems we consider the input-output analysis described in section II C. First, we introduce a harmonic forcing in the momentum equation $\mathbf{f} = \hat{\mathbf{f}}e^{\mathrm{i}\omega t}$; the asymptotic response $\mathbf{x} = \hat{\mathbf{x}}e^{\mathrm{i}\omega t}$ is then given by $\hat{\mathbf{x}} = \mathsf{R}(\omega)\mathsf{B}\hat{\mathbf{f}}$ with

$$\mathsf{R}(\omega) = (\mathsf{M}e^{\mathrm{i}\omega\Delta t} + \mathsf{C} + \mathsf{K}e^{-\mathrm{i}\omega\Delta t})^{-1}\ \frac{e^{\mathrm{i}\omega\Delta t} - 1}{\mathrm{i}\omega}. \tag{46}$$

The matrix $\mathsf{R}(\omega)$ is the resolvent operator and the matrix B is defined such that the forcing terms are only introduced in the momentum equation. For a given angular frequency ω we then maximize the gain by optimizing over all harmonic forcings $\hat{\mathbf{f}}$; this optimal gain can be expressed in terms of the singular value decomposition of $\mathsf{R}(\omega)\mathsf{B}$ according to

$$G^*(\omega) = \max_{\hat{\mathbf{f}}} \frac{\|\mathsf{R}(\omega)\mathsf{B}\hat{\mathbf{f}}\|}{\|\hat{\mathbf{f}}\|} = \|\mathsf{R}(\omega)\mathsf{B}\| = \sigma_1(\mathsf{R}(\omega)\mathsf{B}), \tag{47}$$

with σ_1 denoting the leading singular value. As before, the computational cost associated with the above calculation can be simplified by exploiting the block-circulant structure of

the resolvent operator. We thus compute optimal gain G^* as

$$G^*(\omega) = \max_j \|\hat{\mathsf{R}}_j(\omega)\hat{\mathsf{B}}_0\| \tag{48}$$

where

$$\hat{\mathsf{R}}_j(\omega) = \left(\hat{\mathsf{M}}_j e^{\mathrm{i}\omega\Delta t} + \hat{\mathsf{C}}_j + \hat{\mathsf{K}}_j e^{-\mathrm{i}\omega\Delta t}\right)^{-1} \frac{e^{\mathrm{i}\omega\Delta t} - 1}{\mathrm{i}\omega} \qquad \text{and} \qquad \hat{\mathsf{B}}_0 = \begin{pmatrix} \mathsf{I} \\ 0 \end{pmatrix}. \tag{49}$$

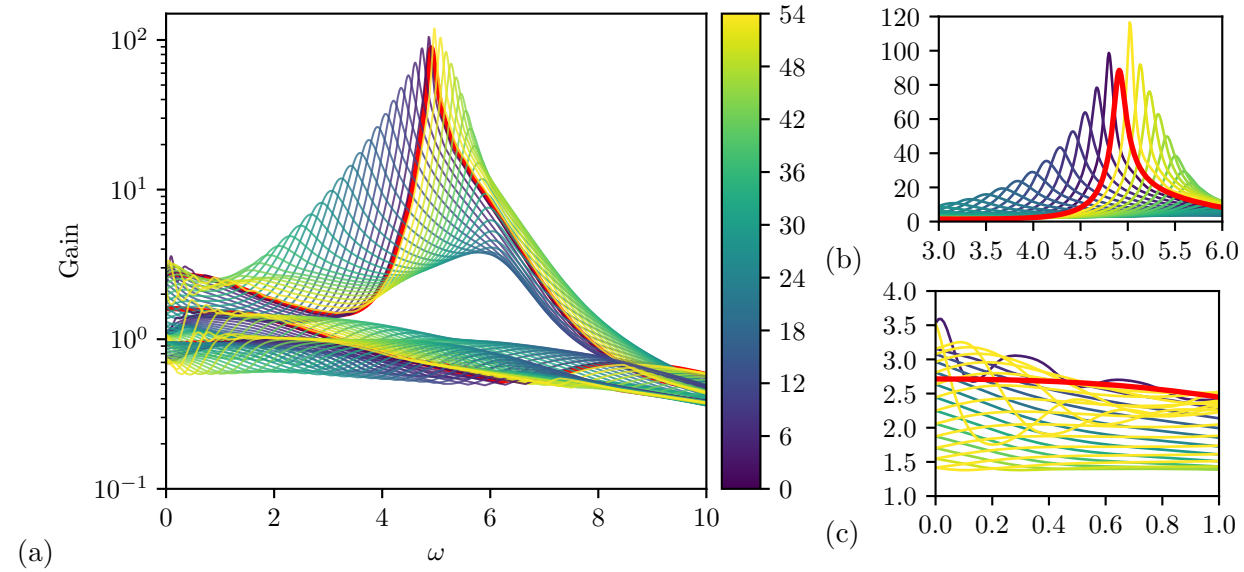

FIG. 11. Optimal gains for varying angular frequency. The curves have been colored according to their corresponding root of unity. The optimal gain for $j = 0$ is displayed in red. In (b) and (c) a closer view is presented, respectively, in the range of amplified wake instabilities and low-frequency dynamics.

In figure 11, we present the singular values of the operator $\hat{\mathsf{R}}_j(\omega)\hat{\mathsf{B}}_0$ as a function of the angular frequency ω. The singular values for the fully periodic case, i.e., $j = 0$, are indicated in red, whereas the remaining curves are colored according to their corresponding root of unity: the case $j = 1$ is shown in dark blue, the case $j = 53$ in yellow; starting from these two cases, the color scheme for higher and lower values of j gradually tends to green. It is apparent from the figure that the maximum amplification at most frequencies is reached for cases that are not purely periodic; only at rather narrow frequency windows ($\omega \approx 9.5$, $\omega \approx 4.9$, $\omega \approx 0.85$ and $\omega \approx 0.55$) does response behavior with single-sub-unit periodicity (i.e., with $j = 0$) constitute the optimal gain to harmonic forcing.

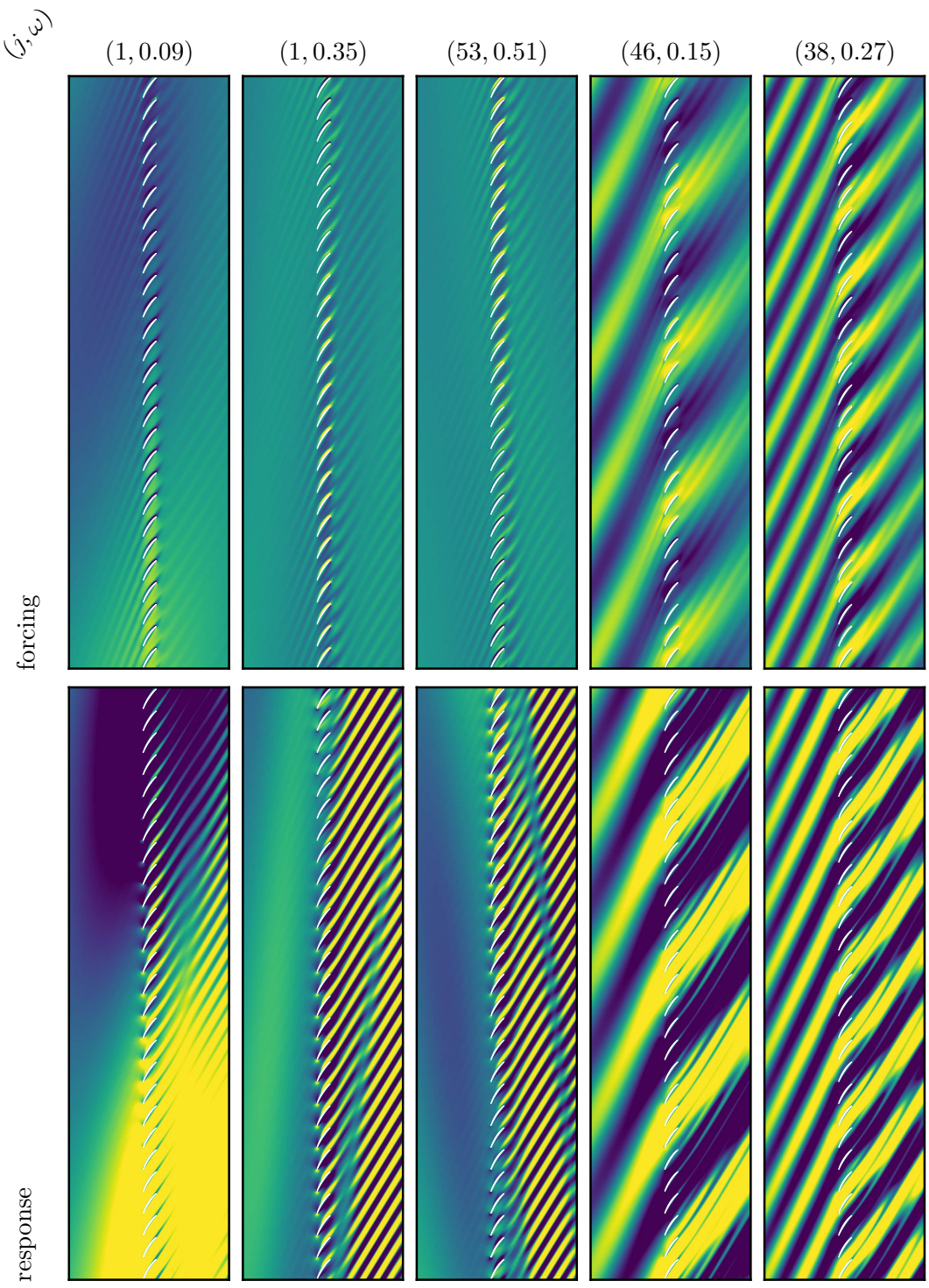

FIG. 12. Optimal forcing and response flow fields from a nonmodal resolvent analysis of a 54-periodic linear blade cascade for selected (low) frequencies. The periodicity j, at which the maximal gain has been obtained, is indicated on top of the subplots, together with the chosen forcing frequency.

Exploring the lower frequencies more closely, we recover the optimal forcing $\hat{\mathbf{f}}$ and resulting optimal response $\hat{\mathbf{x}}$ in the 54-blade linear cascade for a given frequency. This is accomplished using the singular value decomposition of the sub-unit matrices $\hat{\mathsf{R}}_j(\omega)\hat{\mathsf{B}}_j$: the principal singular vectors, evaluated for the value of j that constitutes the maximal gain $G^*(\omega)$, represent the spatial fields of the optimal harmonic input and output structures, once they have been restored to the global domain using (18). For selected low frequencies they are displayed in figure 12.

As the maximal gain for a given frequency is achieved for different values of j, the associated spatial structures reflect the respective periodicity along the linear 54-blade cascade. For a very low forcing frequency of $\omega = 0.09$ the $(j = 1)$-subproblem constitutes the maximum response of the 54-periodic system, and both the forcing and the response are characterized by a modulation along the transverse direction that links and synchronizes the motion across many blades. This modulation, on top of a blade-geometry induced periodicity, is clearly visible in figure 12 for $(j, \omega) = (1, 0.09), (1, 0.35)$ and $(53, 0.51)$, in particular in the response fields. This multi-periodic trend is continued for higher frequencies, as shown in figure 12 for $(j, \omega) = (46, 0.15)$ and $(38, 0.27)$, where synchronized groups of four and two blades, respectively, dominate the optimal forcing and response flow fields. In this case, the 1-periodic structures induced by the blade geometry are far less discernible.

From this analysis, it can be concluded that forcing at low frequencies favors and induces large-scale motion that yields a locked dynamics across multiple blade passages, resulting in traveling structures with transverse wavelengths that exceed the periodicity imposed by the blade geometry.

As we progress to higher forcing frequencies, the appearance of periodicity other than the one associated with $j = 0$ is still noticeable, although to a lesser extent. Figure 13 depicts a selection of optimal forcing and response structures for frequencies above $\omega \approx 0.5$. For the frequencies $\omega = 0.52, 1.75$ and 2.59 (with associated optimal root-of-unity values of $j = 30, 46$ and again 30) we observe a clear lower-frequency modulation imposed on the periodic structures forced by the blade geometry. For a forcing frequency of $\omega = 4.91$ we obtain a fully periodic $(j = 0)$ structure; however, the range of frequencies where this structure is dominant is rather narrow, as can be seen in figure 11. For slightly larger (or smaller) frequencies, periodicities other than the $(j = 0)$-case are favored, even though their contribution to the forcing and response flow field is smaller (see the rightmost panel in

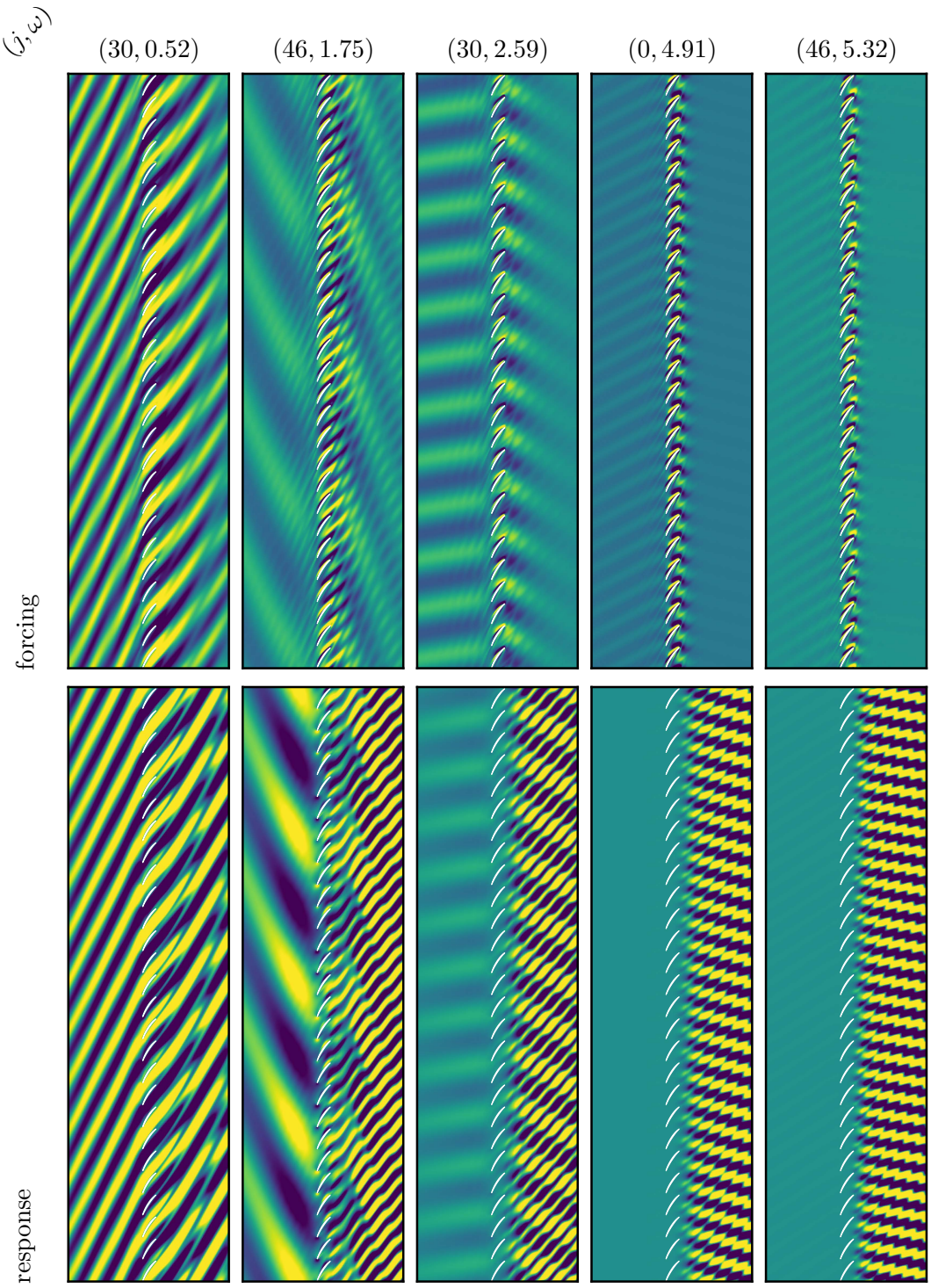

FIG. 13. Optimal forcing and response flow fields from a nonmodal resolvent analysis of a 54-periodic linear blade cascade for selected (higher) frequencies. The periodicity j, at which the maximal gain has been obtained, is indicated on top of the subplots, together with the chosen forcing frequency.

figure 13 for $(j, \omega) = (46, 5.32)$).

IV. CONCLUSIONS

A computational framework for the analysis of fluid systems that consist of n identical units with nearest-neighbor or global coupling has been presented and demonstrated on a range of problems. This framework is based on the fact that the block-circulant nature of the global system matrices yields simplified expressions and associated algorithms that only contain matrices that describe the dynamics of a single unit and its coupling to other (identical) units. The analysis of n-periodic fluid systems can thus be formulated and performed efficiently at the cost of single-unit computations and executed in parallel, while still capturing the global dynamics and fluid structures that span multiple sub-units.

While the framework is closely linked to Floquet theory, Bloch-wave methodology and related techniques for modified boundary conditions, it provides simple and efficient techniques that require minimally invasive modifications of computer codes to enable the type of investigations presented in this study. Compact expressions for the analysis of modal and nonmodal flow characteristics, for the response to impulses or to harmonic forcing, for the quantification of input-output behavior and cross-unit dynamics, and for direct-adjoint techniques have been given. They furnish tools for the investigation of fluid systems that contain periodicity in the form of geometric features or as an assembly of identical units.

The framework has been showcased on various problems of increasing complexity, from a simple model problem describing flow along a grooved wall to interacting arrays of wakes (as for example encountered in heat exchangers), to the incompressible flow through a linear blade cascade. The full set of tools has been applied, and a common feature of the analyses has been the presence – and often dominance – of large-scale motion that spans more than one sub-unit and would be missed by an analysis that imposes periodic boundary conditions over one sub-unit. For example, the flow over a spanwise array of roughness elements is often modeled by a fundamental computational box that contains one roughness element and enforces periodic boundary conditions in the spanwise direction. Similarly, instabilities that show a preference for a specific spanwise scale are commonly studied by concentrating on a fundamental wavelength in the spanwise direction together with periodic boundary conditions. The examples in this article clearly demonstrate that, in both cases, geometries

that consist of multiple copies of this fundamental computational box could support motion and instabilities that span several sub-units, but that are not captured by a fully periodic assumption across one sub-unit.

It is hoped that the computational techniques presented in this article will help in the proper analysis of n-periodic fluid systems arising in a wide range of applications from science and engineering.

ACKNOWLEDGMENT

We wish to gratefully acknowledge financial support from MINECO through the *Programa Estatal de I+D+i Orientada a los Retos de la Sociedad*, grant number DPI2016-75777-R, AEI/FEDER, UE. The second author (M.F.d.P.) also thanks the Department of Applied Mathematics and Theoretical Physics (DAMTP) of the University of Cambridge where part of this research has been conducted under a David Crighton Fellowship.

---

[1] S.D.M. Adams, R.V. Craster and S. Guenneau, "Bloch waves in periodic multi-layered acoustic waveguides," *Proc. R. Soc. A*, vol. 464, pp. 2669–2692, 2008.

[2] P.R. Amestoy, I.S. Duff, J.-Y. l'Excellent, "Multifrontal parallel distributed symmetric and unsymmetric solvers," *Comp. Meth. in Appl. Mech. and Eng.*, vol. 184(2-4), pp. 501-520, 2000.

[3] C.L. Ball, "Advanced technology impact on compressor design and development: a perspective," NASA Techn. Memorandum TM-102341, 1989.

[4] F. Bloch, "Über die Quantenmechanik der Elektronen in Kristallgittern," *Z. für Phys.*, vol. 52, pp. 555–560, 1929.

[5] G. Campa and S.M. Camporeale, "Prediction of the thermoacoustic combustion instabilities in practical annular combustors," *J. Eng. Gas Turb. and Power*, vol. 136(9), pp. 091504, 2014.

[6] M. Choudhari, F. Li and J. Edwards, "Stability analysis of roughness array wake in a high-speed boundary layer", *AIAA Paper 2009-0170*, 2009.

[7] K. Ekici and K.C. Hall, "Nonlinear analysis of unsteady flows in multistage turbomachines using the harmonic balance technique," *AIAA Paper 2006-0422*, 2006.

[8] J.I. Erdos, E. Alznert and W. McNally, "Numerical solution periodic transonic flow through a fan stage," *AIAA J.*, vol. 15(11), 1977.

[9] F.M. Esquivelzeta-Rabell, B. Figueroa-Espinoza, D. Legendre and P. Salles, "Shearing flow over an idealized wavy surface: Comparison between linear theory and DNS," in: Proc. 3rd Braz. Conf. Boiling, Condensation and Multiphase Flow, 2012.

[10] M. Fosas de Pando, D. Sipp and P.J. Schmid, "Efficient evaluation of the direct and adjoint linearized dynamics from compressible flow solvers," *J. Comp. Phys.*, vol. 231(23), pp. 7739–7755, 2012.

[11] W.B. Gardner, "Energy efficient engine (E3) technology status," *AIAA Paper 1982-1052*, 1982.

[12] X. Garnaud and C.C. Mei, "Bragg scattering and wave-power extraction by an array of small buoys," *Proc. Roy. Soc. Lond. A*, vol. 466, pp. 79–106, 2010.

[13] G.A. Gerolymos and V.C. Chapin, "Generalized expression of chorochronic periodicity in turbomachinery blade-row interaction," *Rech. Aérospat.*, vol. 5, pp. 69–73, 1991.

[14] G.A. Gerolymos, G.J. Michon and J. Neubauer, "Analysis and application of chorochronic periodicity in turbomachinery rotor/stator interaction computations," *J. Propul. Power*, vol. 18, pp. 1139–1152, 2002.

[15] N.K. Ghaddar, K.Z. Korczak, B.B. Mikic and A.T. Patera, "Numerical investigation of incompressible flow in grooved channels. Part 1. Stability and self-sustained oscillations," *J. Fluid Mech.*, vol. 163, pp. 99–127, 1986.

[16] N.K. Ghaddar, M. Magen, B.B. Mikic and A.T. Patera, "Numerical investigation of incompressible flow in grooved channels. Part 2. Resonance and oscillatory heat-transfer enhancement," *J. Fluid Mech.*, vol. 168, pp. 541–567, 1986.

[17] A.K. Gopinath, E. van der Weide, J.J. Alonso and A. Jameson, "Three-dimensional unsteady multi-stage turbomachinery simulations using the harmonic balance technique," *AIAA Paper 2007-0892*, 2007.

[18] R.M. Gray, "Toeplitz and circulant matrices: a review," *Found. Trends in Comm. and Inf. Theory*, vol. 2, no. 3, pp. 155–239, 2006.

[19] L. Hascoët and V. Pascual, "The Tapenade Automatic Differentiation tool: principles, model, and specification," *ACM Trans. on Math. Software*, vol. 39, no. 3, 2013.

[20] L. He, "Fourier methods for turbomachinery applications," *Progr. Aero. Sci.*, vol. 46, pp. 329–341, 2010.

[21] V. Hernandez, J.E. Roman and V. Vidal, "SLEPc: a scalable and flexible toolkit for the solution of eigenvalue problems," *ACM Trans. Math. Softw.*, vol. 31(3), pp. 351–362, 2005.

[22] M.R. Jovanovic and B. Bamieh, "Componentwise energy amplification in channel flows," *J. Fluid Mech.*, vol. 534, pp. 145–183, 2005.

[23] H.D. Li and L. He, "Single-passage solution of three-dimensional unsteady flows in a transonic fan rotor," *Proc. Inst. Mech. Eng., Part A: J. Power and Ener.*, vol. 215, pp. 653–662, 2001.

[24] H.D. Li and L. He, "Single-passage analysis of unsteady flows around vibrating blades of a transonic fan under inlet distortion," *ASME J. Turbomach.*, vol. 124, pp. 285–292, 2002.

[25] P. Luchini and A. Bottaro, "Adjoint equations in stability theory," *Ann. Rev. Fluid Mech.*, vol. 46, pp. 493–517, 2014.

[26] J. Martins, P. Sturdza and J. Alonso, "The complex-step derivative approximation," *ACM Trans. Math. Softw.*, vol. 29(3), pp. 245–262, 2003.

[27] V. Mehrmann and H. Voss, "Nonlinear eigenvalue problems: A challenge for modern eigenvalue methods," *GAMM Mitteil.*, vol. 27(2), pp. 121–152, 2004.

[28] G.A. Mensah, G. Campa and J.P. Moeck, "Efficient computation of thermoacoustic modes in industrial annular combustion chambers based on Bloch-wave theory", *ASME J. Eng. Gas Turbines and Power*, vol. 138, pp. 081502-1, 2016.

[29] J.P. Moeck, M. Paul and C.O. Paschereit, "Thermoacoustic instabilities in an annular Rijke tube," *ASME paper* GT2010-23577, 2010.

[30] M. Olaussona, L.-E. Eriksson and S. Baralon, "Evaluation of nonlinear rotor wake/stator interaction by using time domain chorochronic solver," *Proc. 8th Int. Symp. Exp. Comp. Aerothermodyn. Internal Flows*, Lyon, 2007.

[31] S. Patil, T. Sedalor, D. Tafti, S. Ekkad, Y. Kim, P. Dutta, H.-K. Moon and R. Srinivasan, "Study of flow and convective heat transfer in a simulated scaled up low emision annular combustor," *J. Thermal Sci. Eng. Appl.*, vol. 3(11), 2011.

[32] J. Peter and R.P. Dwight, "Numerical sensitivity analysis for aerodynamic optimization: a survey of approaches," *Comp. & Fluids*, vol. 39, pp. 373–391, 2010.

[33] C.S. Peskin, "The immersed boundary method," *Acta Numerica*, vol. 11, pp. 1–39, 2002.

[34] D.S.G. Pollock, "Circulant matrices and time-series analysis," *Queen Mary Univ. London, Dept. Econ.*, Working Paper No. 422, 2000.

[35] A.M. Roma, C.S. Peskin and M.J. Berger, "An adaptive version of the immersed boundary method," *J. Comp. Phys.*, vol. 153 n. 2, pp. 509–534, 1999.

[36] P.J. Schmid, "Nonmodal stability theory," *Ann. Rev. Fluid Mech.*, vol. 39, pp. 129–162, 2007.

[37] P.J. Schmid and D.S. Henningson, "Stability and transition in shear flows," Springer-Verlag New York, 2001.

[38] G. Staffelbach, L.Y.M. Gicquel, G. Boudier and T. Poinsot, "Large eddy simulation of self excited azimuthal modes in annular combustors," *Proc. Comb. Inst.*, vol. 32, pp. 2909–2916, 2009.

[39] S.R. Stow and A.P. Dowling, "Modelling of circumferential modal coupling due to Helmholtz resonators," *ASME paper* GT2003-38168, 2003.

[40] J. Szumbarski, "Instability of viscous incompressible flow in a channel with transversely corrugated walls," *J. Theor. Appl. Mech.*, vol. 45, no. 3, pp. 659–683, 2007.

[41] K. Taira and T. Colonius, "The immersed boundary method: a projection approach," *J. Comp. Phys.*, vol. 225, pp. 2118–2137, 2007.

[42] G.J. Tee, "Eigenvectors of block circulant and alternating circulant matrices," *Res. Lett. Inf. Math. Sci.*, vol. 8, pp. 123–142, 2005.

[43] F. Tisseur and K. Meerbergen, "The quadratic eigenvalue problem," *SIAM Rev.*, vol. 43(2), pp. 235–286, 2001.

[44] L.N. Trefethen and M. Embree, "Spectra and Pseudospectra: The Behavior of Non-Normal Matrices and Operators" *Princeton University Press*, 2005.

[45] P. Wolf, G. Staffelbach, A. Roux, L.Y.M. Gicquel, T. Poinsot and V. Moureau, "Massively parallel LES of azimuthal thermo-acoustic instabilities in annular gas turbines," *C.R. Mecanique*, vol. 337, pp. 385–394, 2009.